

PHENOMENOLOGY OF HIGH OZONE EPISODES IN NE SPAIN

Xavier QUEROL¹, Gotzon GANGOITI², Enrique MANTILLA³, Andrés ALASTUEY¹, María Cruz MINGUILLÓN¹, Fulvio AMATO¹, Cristina RECHE¹, Mar VIANA¹, Teresa MORENO¹, Angeliki KARANASIOU¹, Ioar RIVAS¹, Noemí PÉREZ¹, Anna RIPOLL¹, Mariola BRINES¹, Marina EALO¹, Marco PANDOLFI¹, Hong-Ku LEE⁴, Hee-Ram EUN⁴, Yong-Hee PARK⁴, Miguel ESCUDERO⁵, David BEDDOWS⁶, Roy M. HARRISON⁶⁺, Amelie BERTRAND⁷, Nicolas MARCHAND⁷, Andrei LYASOTA⁸, Bernat CODINA⁸, Miriam OLID⁸, Mireia UDINA⁸, Bernat JIMÉNEZ⁸, Rosa M. SOLER⁸, Lucio ALONSO², Millán MILLÁN³, Kang-Ho AHN⁴

¹ Institute of Environmental Assessment and Water Research, IDAEA-CSIC, C/ Jordi Girona 18-26, 08034 Barcelona, Spain

² Escuela Técnica Superior Ingeniería de Bilbao, Departamento Ingeniería Química y del Medio Ambiente, Universidad del País Vasco UPV/EHU, Urkixo Zumarkalea, S/N, 48013 Bilbao, Spain

³ Centro de Estudios Ambientales del Mediterráneo, CEAM, Unidad Asociada al CSIC, Parque Tecnológico C/ Charles R. Darwin, 14 46980 Paterna, Valencia, Spain

⁴ Department of Mechanical Engineering, Hanyang University, Ansan 425-791, Republic of Korea

⁵ Centro Universitario de la Defensa de Zaragoza, Academia General Militar, Ctra. de Huesca s/n, 50090 Zaragoza, Spain

⁶ Division of Environmental Health & Risk Management, School of Geography, Earth & Environmental Sciences.

University of Birmingham. Edgbaston, Birmingham B15 2TT, UK

⁷ Aix Marseille Univ, CNRS, LCE, 13331 Marseille, France

⁸ Department of Astronomy and Meteorology, Faculty of

Department of Astronomy and Meteorology, Faculty of Physics, University of Barcelona, Martí i Franqués 1, 08028 Barcelona, Spain

Barcelona, Spain

Also at: Department of Environmental Sciences/Centre for Excellence in Environmental Studies, King Abdulaziz University, Jeddah, Saudi Arabia.

ABSTRACT

Ground level and vertical measurements (performed using tethered and non-tethered balloons), coupled with modelling, of ozone (O_3), other gaseous pollutants (NO, NO_2 , CO, SO_2) and aerosols were carried out in the plains (Vic Plain) and valleys of the northern region of the Barcelona Metropolitan Area (BMA) in July 2015; an area typically recording the highest O_3 episodes in Spain. Our results suggest that these very high O_3 episodes were originated by three main contributions: (i) the surface fumigation from high O_3 reservoir layers located at 1500-3000 m a.g.l. (according modelling and non-tethered balloon measurements), and originated during the previous day(s) injections of polluted air masses at high altitude; (ii) local/regional photochemical production and transport (at lower heights) from the BMA and the surrounding coastal settlements, into the inland valleys; and (iii) external (to the study area) contributions of both O_3 and precursors. These processes gave rise to maximal O_3 levels in the inland plains and valleys northwards from the BMA when compared to the higher mountain sites. Thus, a maximum O_3 concentration was observed within the lower tropospheric layer, characterised by an upward increase of O_3 and black carbon (BC) up to around 100-200 m a.g.l. (reaching up to $300 \mu\text{g}/\text{m}^3$ of O_3 as a 10-s average), followed by a decrease of both pollutants at higher altitudes, where BC and O_3 concentrations alternate in layers with parallel variations, probably as a consequence of the atmospheric transport from the BMA and the return flows (to the sea) of strata injected at certain heights the previous day(s). At the highest altitudes reached in this study with the tethered balloons (900-1000 m a.g.l.) during the campaign, BC and O_3 were often anti-correlated or unrelated, possibly due to a prevailing regional or even hemispheric contribution of O_3 at those altitudes. In the central hours of the days a homogeneous O_3 distribution was evidenced for the lowest 1km of the atmosphere, although

47 probably important variations could be expected at higher levels, where the high O₃ return strata
48 are injected according to the modelling results and non-tethered balloon data.

49 Relatively low concentrations of ultrafine particles (UFP) during the study, and nucleation episodes
50 were only detected into the boundary layer.

51 Two types of O₃ episodes were identified: Type A) with major exceedances of the O₃ information
52 threshold (180 µg/m³ on an hourly basis) caused by a clear daily concatenation of local/regional
53 production with accumulation (at upper levels), fumigation and direct transport from the BMA
54 (closed circulation); and Type B) with regional O₃ production without major recirculation (neither
55 fumigation) of the polluted BMA/regional air masses (open circulation), and relatively lower O₃
56 levels.

57 To implement potential O₃ control and abatement strategies two major key tasks are proposed: (i)
58 meteorological forecasting, from June to August, to predict recirculation episodes so that NO_x and
59 VOCs abatement measures can be applied before these episodes start; (ii) sensitivity analysis with
60 high resolution modelling to evaluate the effectiveness of these potential abatement measures of
61 precursors for O₃ reduction.

62 **Keywords:** O₃, photochemistry, air pollution, air quality, NO_x

63

64 INTRODUCTION

65 Ozone (O₃) is an airborne secondary pollutant that is produced through the photo oxidation of
66 volatile organic compounds (VOCs) in the presence of nitrogen oxides (NO_x=NO+NO₂), with more
67 intensive production in high insolation regions. It is well known that its formation processes are
68 very complex and that the reaction and production rates are not linear (Monks et al., 2015 and
69 references therein). According to EEA (2015) 97% of the European population is exposed to O₃
70 concentrations that exceed the WHO guideline (see below) for the protection of the human
71 health. The complexity of this pollutant is also reflected in its air quality targets; thus, the
72 European air quality directive 2008/50/EC establishes a number of O₃ target values (which are not
73 legally binding, as opposed to the limit values set for the majority of pollutants):

- 74 • A human health target value fixed at 120 µg/m³ as 8 hours maxima in a day that should
75 not be exceeded in more than 25 days/year as a three-year mean. This target value was
76 (arbitrarily) increased from the recommended 100 µg/m³ in the WHO air quality guidelines
77 (where no specific number of exceedances is recommended).
- 78 • A population information hourly threshold of 180 µg/m³.
- 79 • A population alert hourly threshold of 240 µg/m³.
- 80 • A vegetation protection target, AOT40 [expressed in µg/m³·h], as the sum of the excess of
81 hourly concentrations above 80 µg/m³ along a given period using only hourly values
82 measured between 8:00 and 20:00 h, Central Europe Time (CET), for every day. Hourly
83 AOT40 from May to July should not exceed 18.000 µg/m³·h O₃ as a mean for 5 years.

84 NO_x has a catalytic effect in O₃ generation, and is only removed from the system by either
85 deposition or oxidation to nitric acid (HNO₃) and reaction with VOCs to yield secondary aerosols,
86 such as inorganic and organic nitrates, which may sequester a significant fraction of NO_x.
87 Consequently, O₃ generation involves not only local and regional air masses but also long-range
88 transport. Thus, as a general observation, long range transport of O₃ and its precursors influence
89 markedly the background O₃ levels in Europe (UNECE, 2010; Doherty et al., 2013). However, this

90 situation might be very different when considering the high summer O_3 episodes of Southern
91 Europe (e.g. Millán et al., 1997, 2000; Palacios et al., 2002; Castell et al., 2008a, 2008b, 2012; Stein
92 et al., 2005; Escudero et al., 2014; Pay et al., 2014; Querol et al., 2016).

93 In the Western Mediterranean basin the problem of tropospheric O_3 has been intensively studied
94 since the early 1980s (Millán et al., 1991, 1996a, 1996b, 1996c, 2000, 2002; Millán, 2002a; Millán
95 and Sanz, 1999; Mantilla et al., 1997; Salvador et al., 1997, 1999; Gangoiti et al., 2001; Stein et al.,
96 2004, 2005; Doval et al., 2012; Castell et al., 2008a, 2008b, 2012; Escudero et al., 2014). Results
97 have evidenced that (i) the meteorology driving O_3 fluctuation in this region is markedly influenced
98 by a very complex orography with high mountain chains surrounding the basin; (ii) in summer, the
99 lack of a marked synoptic advection caused by the presence of the Azores anticyclone and the
100 Iberian and north African thermal lows, together with the sea and land breezes, give rise to air
101 mass recirculation episodes (lasting for several days); and (iii) during these summer vertical and
102 horizontal recirculations of air masses loaded with O_3 precursors and coinciding with high
103 insolation and elevated biogenic VOCs (BVOCs) emissions (Seco et al., 2011), high O_3
104 concentrations may be recorded.

105 Millán's team results demonstrated that Western Mediterranean basin dynamics are very
106 different from those in Central Europe. The latter are dominated by neutral-cloudy conditions,
107 where O_3 episodes are usually associated with advection, and transformation takes place within
108 large displacements of air masses. There, morning fumigation from a high O_3 residual (and
109 stratified) boundary layer (BL) formed over the previous days, in addition to local formation in the
110 sunny midday period may give rise to peak O_3 episodes if conditions persist after several days. In
111 contrast, vertical re-circulations developed over all Western Mediterranean coastal areas,
112 determine a very different O_3 dynamics. Air masses travel all the way from the sea to the
113 continental divide, or to the top of the Apennines in the case of Italy. These air mass circulations
114 create layers over the sea at various altitudes, with accumulated pollutants/precursors in several
115 stages of transformation. These processes can occur during a few consecutive days (e.g. 10 days,
116 Millán et al., 1997). The layers already over the basin descend from 1000-3500 m a.s.l. during the
117 day and can reach the lower levels, providing a high background O_3 to coastal cities when the sea
118 and up-slope breezes build up (Millán et al., 2000). Layers, by definition, are stratified and
119 decoupled from each other so they can move in different directions and speeds at their own
120 heights.

121 Rodriguez et al. (2002) and Cusack et al. (2013) showed that these high background O_3 episodes
122 are characterised also by high particulate matter (PM) concentrations, mostly due to the
123 formation of secondary organic and inorganic aerosols. Such episodes are very common from June
124 to August, and are usually limited by the occurrence of episodic Atlantic or African advective
125 conditions that help (especially the first) to ventilate the Western Mediterranean basin. Minguillón
126 et al. (2015) demonstrated also the occurrence of very intense aerosol nucleation episodes under
127 high insolation scenarios in the vertical column (from 200 to 1000 m.a.s.l.) over the city of
128 Barcelona. As the surface air ascends, aerosols are diluted and levels of O_3 are expected to
129 increase.

130 The Barcelona Metropolitan Area (BMA) is a highly industrialised and dense urban agglomeration
131 extending over the Mediterranean side of northeast Spain. High anthropogenic NO_x and VOCs
132 emissions arise both from road (and shipping) traffic and power generation, which combined with
133 BVOCs emissions, very often cause severe O_3 episodes in the northern plains and valleys (Toll and
134 Baldasano, 2000; Barros et al., 2003; Gonçalves et al., 2009; Seco et al., 2011; Valverde et al.,
135 2016; Querol et al., 2016). The urban plume is transported inland by sea breezes, heading North

136 channelled by N-S valleys that cross the coastal and pre-coastal Catalan Ranges to an intra-
137 mountain plain (the Vic Plain) where the cities of Manlleu, Vic and Tona lie, 40-65 km north of
138 Barcelona (Figure 1). A mean of 15 annual exceedances of the hourly O₃ information threshold/site
139 are recorded at the urban background monitoring sites of these cities (Querol et al., 2016). In
140 2015, 96 out of the 115 hours exceeding the O₃ information threshold in the whole Catalonia air
141 quality monitoring network were recorded in the area within 40-90 km north of Barcelona
142 (towards the Pyrenees), and 82 in the Vic Plain itself
143 (<http://www.gencat.cat/mediamb/qaire/ciozo.htm>).

144 This work focuses on an intensive campaign on O₃ and particulate pollutants performed in and
145 around the BMA during July 2015, when high O₃ episodes were recorded, with the aim of
146 investigating the origin of the most intense O₃ events in north-eastern Spain. To this end, regional
147 air quality monitoring network data, passive dosimeters at ground level, vertical profile
148 measurements of O₃ and ultrafine particles (UFP) in the Vic Plain, and modelling tools were
149 employed.

150

151 **METHODOLOGY**

152 **Study area**

153 This study is set in central Catalonia (Figure 1), in north-eastern Spain. The mountain ranges
154 surrounding the area (Pyrenees and Catalan Coastal Ranges) protect the area from the advection
155 of Atlantic and continental air masses but hamper dispersion of pollutants. The typical winds in the
156 region are the Tramontana (northern winds), the Mistral or Cierzo (north-western winds
157 channelled by the Ebro valley) and the sea breezes in the coastal region. In summer, daytime up-
158 slope winds combined with sea breezes may result in air masses penetrating 120-160 km inland
159 that are injected aloft the top of the mountains, and follow the return night flows towards the sea
160 (Millán, 2014). This scenario of air mass regional recirculation during periods of several days
161 prevails in summer (Millán et al., 1997 and 2000). Hence, summer pollution events are
162 characterised by (i) the absence of large-scale forcing and the predominance of mesoscale
163 circulations; (ii) the formation of a thermal low at a peninsular level (forcing the convergence of
164 surface winds from the coastal areas towards the central plateau with strong levels of subsidence
165 over the Western Mediterranean basin); and (iii) combined breeze dynamics, resulting in the
166 recirculation and accumulation of pollutants over the whole Western Mediterranean basin,
167 including the Eastern Iberian peninsula (Millán 2014 and Millán et al., 1997, 2000).

168 The region is characterised by important atmospheric pollutant emissions from road traffic,
169 industries, biomass burning, livestock, and airport and shipping activities, which coupled with high
170 solar radiation turns into a high rate of secondary PM and O₃ formation (Rodriguez et al., 2002).
171 Industrial activities are mostly concentrated in the Barcelona and Tarragona provinces, and include
172 19 combustion/energy plants, 84 metallurgy plants and 70 mineral industries. Road traffic, airport
173 and shipping emissions are concentrated in the Barcelona area with >3.5 10⁶ vehicles (0.6 per
174 inhabitant, with high diesel and motorbike proportions; DGT, 2014), >45 10⁶ tons of shipping
175 transportation, and >37 10⁶ aircraft passengers in 2014 (Ajuntament de Barcelona, 2015).

176 Agriculture, livestock and biomass burning emissions are spread over the rural areas but
177 concentrated in the core study area, the Vic Plain: a 30 km long depression in the north-south
178 direction located 60 km to the north of Barcelona. The area is surrounded by mountains and it is

179 affected by thermal inversions during the night. The summer atmospheric dynamics dominated by
180 sea breezes from the southern sector, channelled through the valleys formed by the coastal
181 ranges, giving rise to the transport of pollutants from the BMA and the numerous surrounding
182 highways.

183

184 **Ground level measurements**

185 *Online measurements of gaseous pollutants*

186 Measurements of gaseous pollutants were performed at 48 sites belonging to the regional air
187 quality network (Figure 1, XVPCA; <http://dtes.gencat.cat/icqa>, Table S1) from 01 to 31/07/2015.
188 Continuous measurements of O₃, NO, NO₂, CO and SO₂ were carried out using MCV 48AV UV
189 photometry analysers, Thermo Scientific chemiluminescence analysers (42i-TL), Teledyne 300 EU
190 Gas filter correlation analysers; and Teledyne 100 EU UV fluorescence analysers, respectively.

191 *Measurements of gaseous pollutants with passive dosimeters*

192 Diffusion tubes for NO₂ and O₃ sampling (Gradko Environmental) were deployed at 17 locations
193 between the cities of Barcelona and Ripoll (Figure 1) covering strategic areas not monitored by the
194 regional air quality network. The dosimeters were positioned along two main river basins in the
195 study area (Besòs/Congost and Tordera), from the BMA to the Vic Plain. Sampling points were
196 selected avoiding the direct influence of vehicular emissions and located at a height of
197 approximately 2.5 m above ground level. One sample per site and sampling period (01-14 and 14-
198 29/07/2015) were collected. After exposure, samples were stored at 4 °C until analysis.

199 Replicas were placed in 9 locations, showing good reproducibility of the results (relative errors of
200 5%±6% for O₃ and 4%±7% for NO₂). Dosimeters were collocated also at some XVPCA sites for
201 comparison with reference measurements (6 samples for O₃ at Vic (VIC), Montcada (MON) and
202 Montseny (MSY); and 10 samples for NO₂ at Santa María de Palau Tordera (SMPT), Palau Reial
203 (PLR), Tona (TON), Manlleu (MAN), and Granollers (GRA)). Correction factors were obtained from
204 the comparison between dosimeter and reference data (Dosimeter O₃ = 1.01*Reference O₃ +
205 17.43, R² = 0.97; and Dosimeter NO₂ = 1.27*Reference NO₂ + 1.14, R² = 0.90, in all cases in µg/m³)
206 and then applied to the dosimeter data (supplementary information Figure S1).

207 NH₃ passive samplers (CEH ALPHA, Tang et al., 2001) were also used in 30 specific points.

208 *O_x concentrations*

209 O_x values (NO₂+O₃) were calculated to complement the interpretation of O₃ concentrations. The
210 concept of O_x was initially proposed by Kley and Geiss (1994) to analyse the O₃ spatial and time
211 variability by diminishing the effect of titration of O₃ by NO (NO+O₃ → NO₂+O₂, with the
212 subsequent consumption of O₃) in highly polluted areas with high NO concentrations.

213 *Laboratory van in Vic*

214 A laboratory van was deployed next to the Vic air quality station during 10-17/07/2015. Eight-hour
215 PM_{2.5} samples were collected three times per day (00:00-08:00, 08:00-16:00, and 16:00-00:00
216 UTC) by means of Digitel DH80 high volume samplers (30 m³/h) on Pallflex quartz fiber filters (QAT
217 150 UP). Filters were conditioned at 20-25°C and 50% relative humidity over at least 24 h before
218 and after sampling to determine gravimetrically the PM_{2.5} concentration. Subsequently a detailed
219 chemical analysis following the procedure described by Querol et al. (2001) was carried out.

220 Hourly equivalent Black Carbon (BC) in $PM_{2.5}$ concentrations were determined by a multi-angle
221 absorption photometer (MAAP, model 5012, Thermo). PM_1 , $PM_{2.5}$ and PM_{10} hourly concentrations
222 were determined by an optical particle counter (GRIMM 1107).

223

224 **Vertical profiles**

225 During 14-17/07/2015 several vertical profiles up to 1550 m a.s.l. (1000 m a.g.l.) were performed
226 by means of a tethered balloon (details can be found in Table S2) in the city of Vic (Figure 1), at
227 less than 200 m from the laboratory van and the Vic air quality station. The tethered balloon of 27
228 m^3 filled with helium was equipped with an instrumentation pack attached 30 m below the
229 balloon. This setting has been successfully used in previous studies (Minguillón et al., 2015), hence
230 the lack of a fixed support for the instrumentation pack is not expected to hinder the quality of
231 measurements.

232 The instruments included in the pack were:

- 233 • A miniaturized condensation particle counter (Hy-CPC) measuring particle number
234 concentration larger than 3 nm with a time resolution of 1 s and a flow rate of 0.125
235 L/min, using isopropyl alcohol as the working fluid (Lee et al., 2014). The particle number
236 concentration measured by the Hy-CPC will be referred to as N_3 . Prior studies have
237 demonstrated the agreement of the Hy-CPC and conventional TSI CPCs (Minguillón et al.,
238 2015).
- 239 • A miniaturized nano-particle sizer for the determination of the particle number size
240 distribution (Hy-SMPS, Figure S2) in the range 8-245 nm with a time resolution of 45 s and
241 a flow rate of 0.125 L/min (Lee et al., 2015). The instrument output agreed well with the
242 results from a Scanning Mobility Particle Sizer (SMPS, 10-478nm), composed by a
243 Differential Mobility Analyser (DMA, TSI 3081) coupled with a CPC (TSI 3772) (Figure S3,
244 Hy-SMPS= 0.71*Reference SMPS + 999, $R^2 = 0.88$).
- 245 • A miniaturized optical particle counter (Hy-OPC, Figure S2) measuring particle number
246 concentrations in the ranges 0.3-0.5 μm ($N_{0.3-0.5}$), 0.5-1.0 μm ($N_{0.5-1.0}$), 1.0-2.0 μm ($N_{1.0-2.0}$),
247 and 2.0-5.0 μm ($N_{2.0-5.0}$), with a time resolution of 1 s and a flow rate of 1 L/min.
- 248 • A microaethalometer (MicroAeth AE51), which provided BC concentrations derived from
249 absorption measurements on a 5 min basis with a flow rate of 0.15 L/min.
- 250 • A portable O_3 monitor that measures concentrations every 10 s based on UV absorption
251 (POMTM 2B Technologies, Figure S2). The personal POM O_3 monitor was compared with
252 the O_3 concentrations from the nearby reference station, yielding good results ($n=34$ min
253 data; $POM\ O_3 = 0.85 * \text{Reference}\ O_3 + 0.56$, $R^2 = 0.93$) (Figure S1). The measured vertical O_3
254 concentrations reported in this study were normalized to standard temperature and
255 pressure conditions (25 °C, 1013.2 hPa).
- 256 • A Global Position System (GPS).
- 257 • Temperature, relative humidity, pressure, wind direction and wind speed sensors.

258 Moreover, another sounding was carried out on the 16/07/2015 at 11:00 UTC. A free balloon was
259 used with an instrumentation pack equipped with a Hy-CPC, a GPS, a temperature sensor, and a
260 relative humidity sensor. The pack was placed in an insulated box (Figure S4).

262

263 **Meteorological parameters**

264 30-minute meteorological data from 11 sites located throughout the study area in the proximity of
265 air quality monitoring sites were provided by Meteocat (Meteorological Office of Catalonia)
266 (Figure 1 and Table S3). Hourly average wind components were calculated and used in polar plots
267 with hourly O_3 and O_x concentrations, by means of the OpenAir software (Carslaw, 2012). These
268 are bivariate polar plots where concentrations are shown to vary by wind speed and wind
269 direction as a continuous surface.

270

271 **Modelling system for O_3**

272 The ambient O_3 concentrations were modelled using the ARAMIS (A Regional Air Quality Modelling
273 Integrated System) high resolution modelling system that integrates the Weather Research and
274 Forecasting model (WRF-ARW) version 3.1.1 (Skamarock et al., 2008) as a meteorological model,
275 the High Resolution Emission Model (HIREM) (Soler et al., 2004, 2011 and 2015), and the Models-3
276 Community Multiscale Air Quality Modelling System (Models-3/CMAQ) (Byun and Ching, 1999) as
277 a photochemical model. The modelling system was configured using four nested domains, D1, D2,
278 D3, and D4 with horizontal grids of 27, 9, 3 and 1 km, respectively. For the coarser domain, initial
279 and boundary conditions for the meteorological model were taken for the European Centre for
280 Medium-Range Weather Forecast global model (ECMWF) with a $0.5^\circ \times 0.5^\circ$ resolution using
281 nudging and the boundary conditions are forced every 6 h, whilst for the photochemical model
282 initial and boundary conditions model came from a vertical profile supplied by CMAQ itself.
283 Domains are run in one-way nesting and 24 h spin-up was performed to minimize the effects of
284 initial conditions for the inner domains. The output data is saved every hour. ARAMIS is
285 continuously updated, it has been extensively evaluated (Soler et al., 2015) to simulate air quality
286 over regional and local scales. In the present study the domain D3 was used, which covers the area
287 of interest.

288 **RESULTS AND DISCUSSION**

289 **Meteorological background and diurnal cycles of pollutants**

290 Two types of episodes that will be discussed in the following sections were identified concerning
291 the meteorological patterns and the O_3 concentrations recorded.

292

- 293 • Type A episode: Under “usual summer conditions”, with the Azores High located west of
294 Iberia, and a ridge of high pressures extending into southern France, air masses in the
295 Western Mediterranean basin rotate clockwise (anticyclonic) during the day, following the
296 combined sea breezes and upslope flows at eastern Iberia and a simultaneous generalized
297 compensatory sinking is observed in the basin. During nighttime, drainage flows into the
298 sea develop at the coastal strip, subsidence over the basin weakens and the wind over the
299 sea is observed moving southward, transporting the coastal emissions almost parallel to
300 the shoreline (Gangoiti et al., 2001). At the same time, Atlantic gap winds (through the
301 Ebro and Carcassonne valleys), weaken during daytime due to inland sea breezes and
302 become strengthened during nighttime (Millán et al. 1997; Gangoiti et al., 2001, Gangoiti
303 et al., 2006 and Millán 2014). In such conditions, the air layers over the sea in front of
304 Barcelona tend to move within the south-westerlies during the day, following the
305 clockwise rotation, i.e. towards Southern France and the Gulf of Genoa, and within the
northerlies (towards Valencia) during the night. Thus, direct transport of O_3 and precursors

306 from the Fos-Berre-Marseille-Piombino (Livorno) area towards the BMA is weak or null.
307 However, indirect transport is more likely, first into the sea during nighttime conditions,
308 and then following the daytime south-westerlies for the combined coastal sea-breeze and
309 anticyclonic gyre at the coastal strip of Catalonia, which could bring a fraction of the
310 referred O₃ and precursors originated in southern France, together with those emitted at
311 the eastern coast of Iberia

312 • Type B episode: When the anticyclone establishes over Central Europe with relative low
313 pressures to the West over the Atlantic, the flow pattern over the Western Mediterranean
314 changeS: southerly winds blow at height over eastern Iberia, while at ground level, gap
315 winds may weaken or stop the Mistral and the Tramontana winds in the Gulf of Lion, and
316 Barcelona could then be directly affected by O₃ and precursors, coming with the easterlies
317 blowing at the marine boundary layer (emissions from Corsica, Sardinia and Italy).
318 However, under these atmospheric conditions O₃ levels did not reach the observed values
319 found during episodes type A, and the O₃ daily records did not show the classical pattern
320 of accumulation from one day to the next, characteristic of the highest O₃ episodes in the
321 Western Mediterranean (Millán et al., 1997, 2000 and Castell et al., 2008a)

322 Under the above "usual summer conditions", Millán et al. (1991, 1996a, b, c, 1997, 2000, 2002),
323 Gangoiti et al., (2001), and Castell, (2008a) demonstrated the vertical recirculation of O₃-rich
324 masses in the western Mediterranean, with O₃ being formed from precursors transported inland
325 by the combined up-slope and sea breeze winds. O₃ loaded air masses, elevated by topography
326 and sea-mountain breezes will be transported back to the coastal area at a certain altitude during
327 the day and accumulates in elevated stably stratified layers at the coastal areas during the late
328 evening and night. During nighttime and at ground level O₃ depletion dominates mainly in urban
329 and industrial centers, driven by reaction with new emissions, which at the coastal area are
330 transported offshore within the stable surface drainage flows.

331 The synoptic atmospheric situation in July 2015 was characterized by an intense high pressure
332 system over central and southern Europe during almost the whole month (Figure 2). Type A and B
333 scenarios alternated, transporting warm air masses from North Africa towards higher latitudes by
334 the anticyclonic dynamic and reaching extremely high temperatures in Europe. The stagnation of
335 air masses induced a regional meteorological scenario in the area under study, characterized by
336 local/regional re-circulations and sea-land breezes, both channelled by the complex topography.
337 The flow pattern, together with the observed stably stratified layers developed up to a height of
338 2000-2500 m a.s.l. (Figure 3) associated with subsidence, enhanced the accumulation of pollutants
339 and caused several pollution episodes in the north-eastern Iberian Peninsula. Coastal and pre-
340 coastal locations (Barcelona) were mainly affected by daily sea breezes, starting blowing from the
341 east (around 08:00 UTC) and turning progressively to south and southwest. The sea breezes were
342 channelled through the valleys, which are mainly located following a north-to-south axis, and
343 arrived to the monitoring stations predominantly from a southerly direction. However, during the
344 night atmospheric conditions were much more stable with flow patterns dominated by land
345 breezes from N-NW.

346 The VIC site was characterised by stagnant conditions during the day, reaching the maximum wind
347 speed (4 m/s on average) at around 15:00 UTC, when sea-breeze intensity was at the highest
348 (Figure 4). During the night very light winds blew from the north (Figure 4). During the periods 14-
349 20/07/2015 (episode type A) and 03-06/07/2016 (episode type B) the sea breeze blew from 10:00
350 to 18:00 and 10:00 to 21:00 UTC, respectively; but in the first one the wind speed was higher
351 (maximum of 2.7 m/s as an average for the period) and maximal at 14:00 UTC, whereas in the

352 second wind speed was lower, with a maximum mean value for the period of 2.4 m/s at 17:00
353 UTC, but only 1.5 m/s at midday.

354 Averaged ground O₃ concentrations during type A episode recorded at VIC were clearly influenced
355 by these wind patterns, showing a typical midday peak, followed by a higher peak at 13:00-14:00
356 UTC probably caused by the transport of BMA air masses by the breeze (Figure 4). Mean O₃ levels
357 during this A episode reached 195 µg/m³ at 13:00 UTC. During type B episode averaged O₃ levels
358 were also very high (142 µg/m³ at 14:00 UTC) but clearly lower than during the A episode (Figure
359 4).

360 Intensive surface measurements were only available for 10-17/07/2015 (when the mobile
361 laboratory was working at VIC). Average SO₂ levels for this period (included in the type A episode)
362 showed a similar daily pattern to that of O₃ (Figure 4) pointing to a probable Hewson's-type I
363 fumigation process (Hewson, 1964, Geiger et al., 1992) when midday convective flows that abate
364 to the surface a SO₂ rich layer accumulated in the limit of the boundary layer. Ground level
365 concentrations of BC, NO₂ and PM_x showed a similar daily pattern driven by stagnation and traffic
366 rush hour, with maxima concentrations around 06:00 UTC (08:00 h local time, Figure 4). Finally,
367 extremely high concentrations of NH₃ (this is one of the most intensive farming regions of Spain
368 and mean values of the Vic Plain dosimeters reached 30 µg/m³ NH₃ for 01-31/07/2015) followed
369 the typical midday maximum due to evaporative emissions from fertilisers, but the rapid increase
370 of the wind speed and dilution by the growth of the PBL thickness (see vertical profiles of
371 temperature, aerosols and O₃ at VIC in following sections) probably account for a reduction of
372 ground level NH₃ concentrations during the central hours of the day (Figure 4).

373 The varying diurnal and nocturnal air mass patterns in the Vic Plain are also shown by the PM_{2.5}
374 chemical composition. Figure S5 shows the 8-h concentration patterns of selected components
375 during the week period of 10-17/07/2015, including several days (14 to 17/07/2016) of the type A
376 episode defined above, affected by polluted air masses from the BMA.

377 In addition to the regionally transported O₃, concentrations of elemental carbon (EC) and traffic
378 and industry-related metals (including Zn, Cu, Pb, Sn and Sb) were notably enhanced at the end of
379 the week, and were attributed to local sources. This enhancement was most obvious during the
380 00:00-08:00 UTC period (Figure S5), under calm or northerly low wind (drainage slope winds)
381 carrying metallic pollutants from the Cu-smelter located 13 km to the north of Vic, and leading to
382 high Cu, Zn, Sn, W, Pb and Sb concentrations on the nights of 15 and 16/07/2015 (Figure S5). The
383 increase in EC was related to local traffic emissions during the morning rush hour as deduced from
384 the peaking MAAP BC concentrations during 05:00-08:00 UTC (07:00-10:00 h local time), up to 5
385 µg/m³ hourly BC, when compared to 3 µg/m³ recorded as maximum traffic rush hour
386 concentrations in the preceding days (data not shown). In contrast, the rise of organic carbon (OC)
387 concentrations observed during 08:00-16:00 UTC is attributed to the formation of secondary
388 organic aerosols (SOA).

389 Sulphate concentrations did not show any trend, as expected from secondary inorganic
390 components present in relatively homogeneous concentrations on a regional scale, whereas
391 nitrate (and a minor proportion of ammonium) concentrations increased during the 00:00-08:00
392 UTC periods as a result of gas to particle partitioning (Figure S5) due to the thermal instability of
393 ammonium nitrate (Hertel et al., 2012), under typical high daytime temperatures reached in July
394 2015. Interestingly, the stronger southerly winds during the daytime in the second part of the
395 week (see below) appear to have brought polluted air from the BMA as signalled by slightly higher
396 V concentrations (tracer of fuel oil combustion); but also the fumigation from high strata (polluted
397 for air masses that were injected the previous day-s) might account for these SO₂ and V increases.

398 The concentrations of mineral matter and all its components (Al, Fe, Mg, Li, Ti, Rb, Sr, Ti, As) were
399 constant during the week, with relatively higher concentrations in the 08:00-16:00 UTC samples
400 (Figure S5), indicating a higher resuspension caused by stronger afternoon winds. The increment
401 on the 15/07/2015 (08:00-16:00 UTC) was attributed to resuspension of local dust, given that the
402 occurrence of African dust outbreaks was not observed during this period.

403 The free sounding measurements carried out at 11:00 UTC on 16/07/2015 revealed stratified air
404 masses up to 3000 m a.g.l. (Figure 3). The vertical profiles of potential temperature, water vapour
405 and aerosol concentration distributions can be used for the identification of atmospheric layers
406 presenting different properties: a lower layer up to about 1100 m a.g.l. characterised by a relative
407 high aerosol concentration, well mixed and with a relative high and uniform water vapour content.
408 A clear discontinuity between 1100 to 1500 m a.g.l limits the mentioned lower layer and a series
409 of stably stratified layers up to a height of 3000 m a.g.l. This layering of pollutants is probably
410 related to the development of regional and mesoscale convective cells driven by the combined
411 upslope and sea breeze flows developed the day before (Millán et al., 1997).

412

413 **O₃ and O_x episodes**

414 Figure S6 shows the average O₃ and O_x ground level concentrations recorded in July 2015 in the
415 study area at the XPCA air quality monitoring network and with the passive dosimeters. O_x
416 maximum concentrations were recorded at the Vic Plain area and in the coastal sites at the
417 northeast of Barcelona. This may be due to the high O₃ concentrations in Vic and to a higher
418 proportion of primary NO₂ (emitted mainly from diesel engines, and not formed in the atmosphere
419 from NO titration by O₃) in the coastal cities, respectively.

420 In July 2015, the O₃ hourly information threshold was exceeded a total of 74 times at the XPCA
421 stations of Catalonia, 57 taking place in the Vic Plain stations (TON, VIC and MAN), and 69 in the
422 surrounding areas (pre-Pyrenees, High Llobregat river and Montseny).

423 Figure 5 shows hourly O₃ concentrations for the study period from selected monitoring sites. O₃
424 concentrations recorded at a coastal (Begur, BEG; blue, 200 m a.s.l.) and a remote inland western
425 pre-Pyrenean site (MSC, light green, 1570 m a.s.l.) (Figure 5a) show relatively narrow diurnal
426 variations and multiday episodes, with low or enhanced concentrations, according to
427 meteorological fluctuations (accumulation and air mass renovation cycles of 3 to 12 days cause a
428 wider O₃ and O_x concentrations range than the typical daily cycles evidenced in most of the other
429 sites). O₃ variations at the coastal BEG are opposed, in periods such as 01-03, 10-12 and
430 26/07/2015 and several periods from 14-20/07/2015, to those at the inland MSC. As shown by the
431 polar plots from Figure 6, relatively low O₃ concentrations (but still high in absolute terms) were
432 recorded at the BEG coastal site (easternmost site in this figure) when the wind blows from the
433 sea, whereas polluted air masses are transported towards the inland remote MSC (westernmost
434 location in the figure) site under the same meteorological conditions. Conversely, when westerly
435 winds blow, the inland remote MSC site received relatively clean air masses with low O₃ (Figure 6),
436 which are progressively loaded with regional pollution as these are transported towards the
437 coastal BEG site.

438 Data from two urban background sites of Barcelona (PLR and CTL, 81 and 5 m a.s.l., grey and black
439 in Figure 5b) show evidence of a high nocturnal O₃ consumption, with differences due to local NO_x
440 traffic emissions. Following the transport of air masses by combined breezes, the two sites located
441 in the northern periphery of the BMA, along the Besòs river valley (GRA and MON, 140 and 33 m
442 a.s.l., orange and yellow in Figure 5c; 20 and 6 km from BMA in NE and NNE directions, respectively)

443 show local O_3 production, with higher midday concentrations, while very low nocturnal levels
444 reflect again the intensive O_3 consumption (in a densely populated basin). O_3 concentrations were
445 closer between GRA and MON than between the two Barcelona urban sites (PLR and CTL).

446 Relevant O_3 net production and fumigation can be readily seen in the inner Vic Plain (TON, VIC and
447 MAN; 620, 498, 460 m a.s.l.; red, pink and violet in Figure 5d; 45, 55 and 62 km from BMA in a NNE
448 direction, respectively) as well as at the remote eastern pre-Pyrenean site of Pardines (PAR,
449 brown, 1226 m a.s.l, 102 km from BMA in a NNE direction), where O_3 formation and fumigation
450 seems to have already reached its maximum, and similar O_3 concentrations were recorded at all
451 sites during the midday increase. This suggests that the intensity of O_3 formation and fumigation
452 was clearly reduced in the Vic Plain-Pyrenees transect with respect to the Barcelona-Vic Plain (an
453 intermediate production place would be MSY (720 m a.s.l.; green in Figure 7, 39 km from BMA in a
454 NE direction). Polar plots of GRA, TON, MSY, VIC, MAN show clearly that the highest O_3 levels were
455 recorded with wind blowing from the Direction where BMA is located (Figure 6).

456 As it can be observed in Figures 5 and 7, during two periods (01-02 and 07-20/07/2015) O_3
457 concentrations increased progressively from the Barcelona city towards the northern BMA (GRA
458 and MON), the intermediate MSY regional background area and towards the northern Vic Plain
459 sites; and from there it slightly decreased towards the eastern pre-Pyrenees (PAR) following the
460 midday-afternoon combined breeze transport (Figures 5 and 7). During these days, no exceedance
461 of the information threshold was produced in the urban environment; only sporadic
462 measurements above the human protection target value were recorded in the close surroundings
463 of Barcelona. However, frequent exceedances of both thresholds were recorded in a regional
464 transport context towards the north of the BMA.

465 While differences in O_3 concentrations between TON, GRA, MSY, BEG and CTL were observed
466 during the period 03-06/07/2015 (B type episode), O_x concentrations show a very similar behavior
467 along the Vic Plain, both qualitative and quantitative (Figure 7, O_x is not reported at BEG due to
468 the lack of NO_2 measurements). Conversely, in the period 07-20/07/2015 (that includes the A type
469 episode), characterized by a change in the synoptic conditions, differences in daily maximum O_x
470 values resemble the same behavior of O_3 alone, with a positive and marked inland gradient. O_3
471 concentrations at BEG, a coastal site far in the northeast were higher during the former period and
472 showed low intra-day variation, indicating a probable long range transport of polluted air masses
473 (Figure 7).

474 O_3 and O_x concentrations at the regional background site (MSY, 720 m a.s.l., green in Figure 7)
475 depict also the meteorologically influenced patterns (in the sense previously described for BEG
476 and MSC), but with a clear overlapped and pronounced daily fluctuation, with marked higher
477 concentrations indicating O_3 generation from a regional origin, especially on 01-02 and 07-
478 20/07/2015 (Figure 7).

479 Diurnal O_3 concentrations in the Vic Plain (around 460-620 m a.s.l.) were markedly higher than at
480 the coastal (CTL, PLR) sites, and slightly higher than at mountain sites (MSY, PAR and MSC, from
481 720, 1226 and 1570 m a.s.l.) during the 01-02 and 07-20/07/2015 periods. The O_3 hourly
482 information threshold of $180 \mu\text{g}/\text{m}^3$ was exceeded 55 times in the Vic Plain (3 sites), with 50 of
483 these exceedances taking place during 01/07/2015 and 14-20/07/2015. For these exceedances, an
484 hourly contribution of up to $150 \mu\text{g}/\text{m}^3$ of O_x (mostly O_3) both from fumigation of recirculated
485 return layers (injected at an altitude of 1500-3000 m a.g.l. in the prior day(s)), and from transport
486 and photochemical generation of O_3 of the BMA plume, might be estimated based on the
487 differences of the O_x early afternoon maxima recorded at the coastal BMA sites (CTL, PLR) and the
488 ones in the Vic Plain (TON, MON, VIC). Thus, as shown in Figure 7, on 14-18/07/2016 midday

489 maxima recorded at CTL (into BMA) range between 38-62 ppb O_x, on an hourly basis; whereas at
490 TON (in the Vic Plain), these reach 102-115 ppb. Accordingly, differences of 50-73 ppb O_x (close to
491 100-150 $\mu\text{g}/\text{m}^3$ O_x) between CTL and TON can be estimated for these days.

492

493 Type A episode (14-20/07/2015)

494 During this episode, a progressive time shift of the daily hourly O₃ and O_x maxima was observed
495 from the Barcelona area (10:00 UTC, at CTL into the BMA) towards the metropolitan periphery
496 (11:00, at GRA), the intermediate mountain sites (13:00, MSY, 39 km from BMA), the Vic Plain
497 (12:00, 13:00 and 14:00, TON, VIC and MAN, 45, 55 and 62 km from the BMA, respectively) and
498 the northern pre-Pyrenean site (16:00, PAR, 102 km from BMA) (Figure 8). As described above, this
499 variation points to the process of O₃ and O_x formation with a mean O_x difference between the
500 urban-coastal sites and the Vic Plain hourly maxima of up to 73 ppb O_x (around 150 $\mu\text{g}/\text{m}^3$) for the
501 TON site when subtracted O_x hourly maxima from CTL (Figure 7), with a maximum average O₃
502 hourly levels of around 200 $\mu\text{g}/\text{m}^3$. These O_x differences are mostly due to O₃ differences (Figure
503 8). Accordingly, during these intense O₃ pollution episodes, more than 50% of the O_x and O₃ hourly
504 maxima concentrations are attributable to (i) O₃ contributions from the previously referred
505 surface fumigation of recirculated strata (over the VIC-MAN-TON area) containing the polluted air
506 masses injected the day before by complex topographic induced circulations; and to (ii) the local
507 O₃ generation and surface transport of the BMA plume into inland valleys. Attributing these O₃
508 exceedances to local/regional causes is also supported by the spatial distribution of the hourly O₃
509 maxima, the number of hourly exceedances of the information threshold, the time shift of the
510 exceedances at the different sites (as moving towards the north) (Figure 9), and the polar plots of
511 hourly O₃ concentrations pointing towards the BMA as main source region (Figure 6). It is
512 important to note that in the coastal sites the PBL height is markedly reduced when compared
513 with the inland regions and then the capture of these high altitude O₃-rich layers by the PBL
514 growth and the consequent fumigation on the surface is less probable in the coastal areas than in
515 the inland ones.

516 Thus, during the A episode, O₃ has mostly a major local/regional origin (with O_x maximum hourly
517 levels progressively increasing from 166 to 246 $\mu\text{g}/\text{m}^3$ from the BMA to the Vic Plain). The
518 concatenation of daily cycles of regional/long range recirculation of air masses and regional/local
519 O₃ production in the A episode accounted for the accumulation of O_x and the consequent
520 exceedance of the hourly information threshold. Castell et al. (2008a) have already reported a
521 correlation between their 'recirculation factor' (a meteorological parameter devised to increase
522 with the concatenation of days with regional vertical recirculation of air masses) with the
523 occurrence of O₃ episodes in 2003. The relevance of these recirculations in originating these high
524 O₃ episodes in Southern Europe was highlighted already, not only by scientific papers by the
525 CEAM's team but also assumed by the European Commission (EC, 2004).

526 Figures 10 and 11 show results for the vertical profiles (0-1100 m a.g.l.) of O₃ concentrations,
527 particle number concentrations for particles > 3 nm (red), 0.3-0.5 μm (blue), 0.5-1.0 μm (brown),
528 ambient temperature, relative humidity and wind direction, obtained at the beginning of the A
529 type episode (from 14 to 17/07/2015).

530 In the profiles from 07:06 to 08:21 UTC on the 14/07/2015, a boundary layer (150 to 250 m thick)
531 with relatively high levels of N₃ (0.8 to 2.0 10^4 #/cm³) was differentiated from the free troposphere
532 (0.2 to 0.8 10^4 #/cm³) (Figure 10). However, in the profile obtained from 09:42 to 10:52 UTC on
533 17/07/2015, the growth by convective turbulence accounts for a homogeneous boundary layer

534 and profile of $N_{0.3-0.5}$ below 1000 m a.g.l. (Figure 10). Inside the boundary layer nucleation occurred
535 (yellow to red areas in Figure 12 for 16/07/2015) regionally driven by photochemical processes.
536 Minguillón et al. (2015) showed the occurrence of these nucleation events into the mixing layer as
537 convective transport elevates and dilutes air masses from polluted areas under high insolation in
538 Barcelona. During 14-16/07/2015 nucleation episodes occurred occasionally, but only inside the
539 boundary layer. On the 17/07/2015 at 9:42-10:52 UTC new particle formation occurred probably
540 at relatively high altitudes, also inside the boundary layer, as deduced from the high N_3 levels
541 measured from 400 to 1000 m a.g.l., with concentrations reaching $1 \cdot 10^4 \text{#/cm}^3$, while
542 simultaneously low concentrations ($< 0.3 \cdot 10^4 \text{#/cm}^3$) were measured at ground level (Figure 10).
543 This vertical gradient is not observed for the coarser particles ($N_{0.3-0.5}$ and $N_{0.5-1}$) and O_3 (Figures 10
544 and 11, for which relatively constant levels were measured inside the boundary layer), suggesting
545 new particle formation.

546 On 14/07/2015 07:06-08:21 UTC a well stratified atmosphere (Figure 11) with both thermal and O_3
547 layers is observed, with a general upward increasing trend for O_3 from $40 \mu\text{g}/\text{m}^3$ at ground level to
548 much higher levels in different strata, such as one reaching $150 \mu\text{g}/\text{m}^3$ in strata at 500 and others
549 with 140, 100 or $40 \mu\text{g}/\text{m}^3$, such as the ones at 300, 800-1000 or 400 m a.g.l., respectively,
550 reflecting, in addition to stratification of O_3 concentrations in altitude, the effect of surface
551 depletion by NO titration and by deposition during the night (see in Figure 11 the progressive O_3
552 depletion from $150 \mu\text{g}/\text{m}^3$ at 500 m a.g.l. to $40 \mu\text{g}/\text{m}^3$ at surface levels). From 13:49 to 15:03 UTC
553 on the 14/07/2015 (Figure 11) the vertical profile changed substantially, with an already unstable
554 atmosphere near the ground, showing very high surface O_3 concentrations of $217 \mu\text{g}/\text{m}^3$ that
555 increase up to $330 \mu\text{g}/\text{m}^3$ in a layer around 100 m a.g.l., decreasing again through an upper layer
556 with values of $240 \mu\text{g}/\text{m}^3$ until 300 m a.g.l. (where measurements were not available due to
557 instrumental problems). This 100-200 m a.g.l. very high O_3 layer agrees with the modelled O_3
558 concentrations for the study area (Toll and Baldasano, 2000; Barros et al., 2003; Gonçalves et al.,
559 2009) and reflects elevated O_3 concentrations due to local production and transport of O_3 , that
560 decrease from 100 m a.g.l. to the surface due to its titration, consumption and deposition. On 15
561 and 16/07/2015, a similar upward increasing O_3 gradient was observed in the early morning
562 (Figure 12). On 17/07/2015 7:39-08:40 UTC O_3 concentrations were relatively constant, but
563 showing also a strongly stratified profile, in the range of $100-165 \mu\text{g}/\text{m}^3$ in the lower 500 m. In the
564 last profile from 09:42 to 10:52 UTC, O_3 concentrations increased from 140 to $200 \mu\text{g}/\text{m}^3$ from 200
565 to 1000 m a.g.l., but again a maximum close to $200 \mu\text{g}/\text{m}^3$ was observed at the same height
566 around 100 m a.g.l. (Figure 11).

567 Thus, vertical profiles of the type A episode are characterised in the early morning by a strong
568 stratification, showing low ground level O_3 concentrations, due to low production (low insolation)
569 and/or consumption (titration and deposition), and increasing concentrations with altitude. This
570 variation is related to prevailing meteorological conditions enhancing local recirculation or larger
571 scale transport with high O_3 masses injected (the day before) at certain altitudes by vertical
572 recirculations into the residual layer, above the nocturnal surface stably stratified boundary layer.
573 Nevertheless, during specific days, homogeneous O_3 vertical profiles up to 1000 m a.g.l. (the
574 maximum height reached with captive sounding) were also evidenced, but probably not
575 maintained at higher levels (where we were not able to measure with our system). Thus, as shown
576 by the 4500 m profile measured with the free sounding on 16/07/2016 (Figure 3), high PM (and
577 probably O_3) strata are present between 1500 and 3000 m a.g.l., these being probably the polluted
578 air masses injected the day before in the northern mountain ranges and recirculated to the coast at
579 certain altitudes (see modelling outputs below). On the other hand, with constant southerly winds
580 (from the coastal area to the Vic Plain) usually associated with the combined sea-breeze and up-

581 slope flows, O_3 was enriched in the lower 100-200 m atmospheric layer, generated by the
582 intensive local photochemical production. O_3 concentrations reached maximal values (up to 330
583 $\mu\text{g}/\text{m}^3$) on the top of this layer, while they decreased at lower heights by titration and deposition,
584 although hourly levels of 225 $\mu\text{g}/\text{m}^3$ were still recorded. These results are consistent with the
585 gradient of O_3 concentrations between the Vic Plain (around 500 m a.s.l.) and the MSY mountain
586 site (720 m a.s.l., and more close to the sea) during the episodes, (Figures 7 to 9). At higher
587 altitude, O_3 concentrations decreased but were still high (150-240 $\mu\text{g}/\text{m}^3$) due to the O_3 formation
588 in air masses constantly transported from the coastal area, which also incorporates O_3 and
589 precursors recirculated the day before, as it is shown next.

590 Interesting results are also obtained by comparing the vertical profiles of BC and O_3 (Figure 13). BC
591 is a tracer of local primary pollution at ground level, and of the potential transport and
592 stratification of regional/local primary pollutants (together or not with regional O_3) when present
593 at high altitude. On 14/07/2015 07:06-08:21 UTC, at 350 m a.g.l. (and similarly on 15-17/07/2015
594 but at varying heights, 100-350 m a.g.l.) a clear discontinuity is evidenced with sudden and
595 simultaneous decreases of BC and O_3 above these heights. The relatively high BC levels within the
596 lower layer suggest the nocturnal accumulation, while O_3 appears in strata (with low values near
597 the ground due to titration and deposition) and with a high concentration just above that level
598 (350 m), now with low BC concentrations. There is a further upward decrease of BC and an
599 increase of O_3 up to the limit of the sounding (870 m).

600 The occurrence of an O_3 maximum layer around 100-200 m a.g.l., on top of the nocturnal stably
601 stratified boundary layer reinforces the idea of an important local production contributing to an
602 upward increase of O_3 inside the layer. Finally, at the highest altitudes reached in this study (900-
603 1000 m a.g.l.), BC and O_3 concentrations were often anti-correlated or unrelated, possibly more
604 related with aged air masses re-circulated within the whole region and with a mixed origin:
605 including local-to-regional sources, more distant over the W-Mediterranean or even from
606 hemispheric transport of air masses as reported by UNECE (2010).

607 Figure 14 shows mean O_3 hourly concentrations recorded at VIC for the episodes A and B, as well
608 as mean wind speed and direction. Mean hourly concentrations are characterized by an increase
609 until 10:00-11:00 UTC, followed by an inflection point and a more marked increase, with a maxima
610 between 13:00 and 14:00 h UTC, and then a progressive decrease, more marked in the episode A.
611 As stated above, processes contributing to increase levels were attributable to fumigation,
612 photochemical production and transport of high O_3 air masses, all controlled by insolation. Millán
613 et al. (2000) described this characteristic diurnal O_3 pattern typically for inland valley stations (as in
614 our case around 75 km from the coast), where the first O_3 increase is attributed to O_3
615 contributions from surface fumigation of high recirculated return strata as well as from the arrival
616 of higher O_3 air masses transported by sea-breeze and the local photochemical production from
617 precursors. On the other hand, the second O_3 concentration 'hump' is coincident with maximum
618 wind speed and probably corresponds to a more intensified sea breeze transport compared with
619 local photochemical formation and fumigation. Figure 14 shows that the two O_3 increases (and
620 consequently the contributions from the 3 above processes) are more pronounced in the type A
621 compared to the type B episode, and that the second maxima (more associated to inland surface
622 transport by sea breeze) is wider, coinciding with a shift of the maxima wind speed towards the
623 late afternoon, in the B episode.

624 Modelling outputs for the A episode points to light winds from the south, transporting pollutants
625 from the BMA towards northern areas (including the Vic Plain), and triggering the hourly O_3
626 exceedances under the effect of the sea and land breeze transport. Thus, Figures 15 and 16 show

627 the horizontal wind vector at 10 m a.g.l. and NO₂ and O₃ concentrations both at ground level and
628 at a height above the surface layer, at different hours for two representative days of the type A
629 and B episodes, respectively. During the type A episode day (15/07/2015), the effect of the land
630 breeze transport accumulates NO₂ over the sea during the night, starting intense O₃ production
631 when sun rises and sea breezes start the inland transport. Maximum concentrations of O₃,
632 exceeding 180 µg/m³ were calculated by the model and measured at the stations located in the
633 Vic Plain (TON, VIC and MAN, Figure 16), although the model overestimated maximum O₃
634 concentrations in TON and VIC and delayed the hourly maximum value in all stations. The vertical
635 distribution shows an important accumulation of around 110 µg/m³ trapped in a reservoir layer at
636 around 1500 m a.s.l. during the night (Figure 17), which will fumigate downwards into the new
637 developing mixing layer during the following hours. Local O₃ production from fresh precursors
638 accumulated during the night in the stably stratified surface layer and then progressed inland
639 along the midday hours. This results in an O₃ enriched plume within a layer of 1000-1500 m depth
640 in the late afternoon, following the model results (Figure 17). This mixing layer also incorporates
641 O₃ from upper reservoir layers after fumigation during the inland travel. The O₃ located at upper
642 levels can re-circulate back into the sea and it will be potentially available to be transported inland
643 (Millán et al., 1997 and 2002), to re-start a new cycle the following day.
644

645 **Type B episode (03-06/07/2015)**
646 As opposed to episode A, during the type B episode and 22-31/07/2015, despite the high O₃ and
647 O_x concentrations, these concentrations were very similar in the urban and remote coastal sites
648 and all along the northern sites, including the Vic Plain. Hence, the averaged O_x hourly
649 concentrations of all the study sites were close to those at the coastal urban site in Barcelona CTL
650 (and in the case of the O₃ close to the remote coastal site of BEG) compared with the large
651 differences reported for the A episode (Figure 8). The high O_x peak measured at the urban site
652 during the mornings of the B period (Figure 8) and from 8:00 to 10:00 UTC in the average hourly
653 patterns (Figure 9) is due to the contribution of primary NO₂. According to Carslaw et al. (2016) the
654 Euro 1 to Euro 2 diesel engines in Europe (early 1990s) emitted 5-10% of primary NO₂ and 90-95%
655 of NO, whereas the Euro 4 to Euro 5 equivalent engines (2004 and 2009 onwards) emit 16-29% of
656 primary NO₂ and 71-84% of NO.

657 Also as opposed to the A episode, during the B episode, O_x levels varied in a very narrow range
658 from East (coastal) to West (mountains, MSC site) and from South (BMA) to North (Vic Plain) and
659 at different heights (from Barcelona and BEG at sea level to MSC at 1570 m a.s.l.). Following the
660 results of the model in the Figures 15 and 17, O₃ does not re-circulate around the region in this
661 period. There is no accumulation from one day to the next in reservoir layers located over the
662 region. Southerly winds blow at height during the whole period and the combined sea breeze and
663 upslope winds developed at lower layers during daytime, after coupling with the southerlies, vent
664 out the O₃ production and the rest of pollutants to the north. The circulation is open, as opposed
665 to the type A episode, which show a closed circulation (it is never completely closed) (Millán et al.,
666 1997, 2000). Unfortunately, vertical profiles of O₃, UFP, PM and BC profiles were not obtained for
667 this episode.

668 Model outputs also evidence a net night and early morning transport of O₃ at lower layers from
669 east and north-east during the B episode, supporting the hypothesis of a regional transport from
670 Southern France, advecting aged air masses to the whole region, while O₃ and its precursors from
671 the BMA were transported during the morning to the south-west regions (Figure 15) giving rise to
672 hourly O₃ exceedances in some stations situated in this area. Figure 15 also shows that during this
673 episode (03/07/2015) the combined sea-breeze and upslope wind transported O₃ and precursors

674 to the western pre-Pyrenees area, and values lower than 180 $\mu\text{g}/\text{m}^3$ were measured and modelled
675 in all monitoring stations and mainly in the Vic Plain. The vertical distribution of O_3 also shows
676 relatively low concentrations over most of the domain (Figure 17).

677

678 CONCLUSIONS AND IMPLICATIONS FOR AIR QUALITY

679 Very high levels of O_3 were recorded in the plains and valleys of the northern regions surrounding
680 the Barcelona Metropolitan Area (BMA) during July 2015, where 69 out of the 74 exceedances of
681 the hourly O_3 information threshold measured in the entire air quality monitoring network of
682 Catalonia were recorded. This represents a major environmental problem for which air quality
683 managers must implement European and national legislation.

684 Both experimental measurements and modelling exercises suggest that these very intense O_3
685 episodes were originated by the concatenation of daily cycles of vertical recirculation of air masses
686 that accumulated photochemically generated pollutants (Millán et al., 1997, 2000, 2002; Gangoiti
687 et al., 2001 and Castell et al., 2008a, Valverde et al., 2016), favoured by the high BVOCs and
688 anthropogenic NO_x emissions in the BMA region. The lower 1000 m a.g.l. were highly enriched in
689 O_3 by fumigation from precursors and O_3 located at upper levels (1500-3000 m a.g.l.). Additionally,
690 local contributions of O_3 to these episodes were also demonstrated by soundings of the lower
691 layers (0-1000 m a.g.l.). Thus, slightly higher concentrations of O_3 were measured in stations
692 located at the plains and inland valleys than at higher altitudes (up to +30-40/ $\mu\text{g}/\text{m}^3$ added to
693 180 $\mu\text{g}/\text{m}^3$ reached in the mountain sites), due to the local photochemical production from fresh
694 precursors emitted during the night and early morning, and their channelling within the combined
695 upslope and sea breeze circulation that transports O_3 and precursors from the BMA. Thus vertical
696 profiles identified a high O_3 layer at 100-200 m a.g.l., produced by these local processes and also
697 by the high deposition and titration of O_3 at the lower 100m depth layer. In our (mostly rural)
698 study low concentrations of ultrafine particles were recorded at this high O_3 100-200 m a.g.l. layer
699 and nucleation episodes were only detected into the boundary layer, most of the days at the
700 lower atmospheric levels.

701 Two types of high O_3 episodes (A and B) were identified in the area:

702 Type A episode: Characterized by major local/regional O_3 recirculation, fumigation, production and
703 transport, superimposed on the typical regional/long range transport, and by the occurrence of
704 major exceedances of the O_3 information threshold (14-20/07/2015). Surface fumigation from
705 high O_3 return (to the sea) layers injected the day(s) before at altitudes of 1500-3000 m a.g.l., and
706 recirculated over the VIC-TON-MAN area, as well as direct surface transport and formation of
707 local/regional polluted air masses (with O_3 and precursors) from the BMA towards the north,
708 decisively contributed to these exceedances. Thus, this atmospheric scenario is governed by poor
709 ventilation under local breeze circulations and vertical recirculation of air masses over the study
710 area.

711 Type B episode: With a major regional transport O_3 contribution, yielding similar O_x levels at all
712 monitoring sites of the study area, with the arrival of aged air masses from the east/northeast
713 (high O_3 levels entering through the coast), but without major transport from BMA to the Vic Plain
714 (3-6/07/2015), and without vertical recirculation of air masses over the study area. When sunlight
715 activates atmospheric photochemistry in the early morning, the northern regions were loaded
716 with air masses with lower content of O_3 precursors, since air masses were transported from the
717 BMA to the southwest (parallel to the coast) from 00:00 to 09:00 h UTC. The combined breeze at
718 midday favored the transport towards the northwest, rather than to the north, as described for

719 the type A episode. In addition the aged air masses are not vertically recirculated and leave the
720 region towards the north-east (to France). Thus, O_3 concentrations were still relatively high
721 (exceeding $120 \mu\text{g}/\text{m}^3$ but below $180 \mu\text{g}/\text{m}^3$) due to local production from fresh precursors and
722 background O_3 contributions from the western Mediterranean, but not enough to exceed the
723 information threshold.

724 From the perspective of possible precursor abatement strategies, direct mitigation measures at
725 the BMA would have had a minor effect on O_3 concentrations at the Vic Plain area during the type
726 B episode. However, during the type A episode, a reduction of NO_x and/or VOCs emissions in the
727 BMA, some days before and during the episode, might have an effect on O_3 concentrations
728 recorded in the Vic Plain. Nonetheless, due to the non-linearity of the O_3 generation processes,
729 sensitivity analysis with high resolution modelling is necessary to evaluate the possible effects in
730 terms of absolute concentrations.

731 The use of O_x data from strategically selected monitoring sites in the east coast, western and
732 central mountain areas, urban background sites of the BMA and sites in the Vic Plain, tracking the
733 natural routes of pollutant transport, is a useful tool to assess the different regimes leading to high
734 O_3 concentrations, and to differentiate between type A and type B episodes, with important
735 implications in the design of potential abatement strategies.

736 We are aware that we only analysed the most intense O_3 episodes occurring in July 2015, and that
737 there might be other scenarios, different to type A and B, yielding high O_3 events, such as the
738 transport of aged air masses from other regions of Europe or the transport of the BMA emissions
739 in meteorological scenarios different to those described here. However in a recent study (Querol
740 et al., 2016) we demonstrated with the analysis of the 2000-2015 O_3 data series, that the Vic Plain,
741 (40-50 km north of Barcelona) is the area in Spain recording the highest number of annual
742 exceedances of the O_3 information threshold, orders of magnitude higher than the surrounding
743 areas of the axis BMA-Vic Plain-Pre-Pyrenean ranges. Thus it is clear that the BMA emissions and
744 the vertical re-circulations caused by the local complex orography have an important role in the
745 occurrence and development of intensive O_3 episodes in the region.

746 To implement potential (and difficult) abatement strategies two major key tasks are proposed:

- 747 1. Meteorological forecast from June to August to predict recirculation episodes in order to
748 apply abatement measures for O_3 precursors before a recirculation episode starts. As stated
749 above, the relevance of these recirculations in originating these high O_3 episodes in
750 Southern Europe was assumed already by the European Commission in 2004 (EC, 2004).
- 751 2. Sensitivity analysis with high resolution modelling to evaluate the effectiveness of NO_x and
752 VOCs abatement measures on O_3 reduction.

753

754 **ACKNOWLEDGMENTS**

755
756 The present work was supported by the Spanish Ministry of Economy and Competitiveness and
757 FEDER funds under the project HOUSE (CGL2016-78594-R), by the Generalitat de Catalunya
758 (AGAUR 2015 SGR33 and the DGQA). Part of this research was supported by the Korea Ministry of
759 Environment through "The Eco-Innovation project". The participation of University of Marseille
760 and University of Birmingham was partially supported by two TNA actions projects carried out
761 under the ACTRIS2 project (grant agreement No. 654109) financed by the European Union's

762 Horizon 2020 research and innovation program.. The support of the CUD of Zaragoza (project CUD
763 2013-18) is also acknowledged. We are very thankful to the Generalitat de Catalunya for supplying
764 the air quality data from the XPCA stations, to METEOCAT (the Meteorological Office of
765 Catalonia) for providing meteorological data and to the IES J. Callís and the Meteorological Station
766 from Vic for allowing the performance of the vertical profiles and mobile unit measurements,
767 respectively. In memoriam of Andrei Lyasota.

768

769 REFERENCES

770

771 Ajuntament de Barcelona, 2015. Annual Statistics of the Barcelona
772 City.<http://www.bcn.cat/estadistica/catala/dades/anuari/cap15/index.htm>

773 Barros N., Borrego C., Toll I., Soriano C., Jiménez P., Baldasano J.M., 2003. Urban Photochemical
774 Pollution in the Iberian Peninsula: Lisbon and Barcelona Airsheds. *J. Air & Waste Manage.*
775 Assoc. 53:347–359.

776 Byun D.W. and Ching J.K.S., 1999. Science algorithms of the EPA Models-3 Community Multiscale
777 Air Quality (CMAQ) modeling system. National Exposure Research Laboratory, US
778 Environmental Protection Agency, Research Triangle Park, NC: Atmospheric Modelling
779 Division; 27711

780 Carslaw D.C., 2012. The openair manual – open-source tools for analysing air pollution data,
781 Manual for version 0.7-0, King's College, London.

782 Carslaw D.C., Murrells T.P., Andersson J., Keenan M., 2016. Have vehicle emissions of primary NO₂
783 peaked? *Faraday Discussions*, In press DOI: 10.1039/C5FD00162E

784 Castell N., Mantilla E., and Millán M.M., 2008a. Analysis of tropospheric ozone concentration on a
785 Western Mediterranean site: Castellon (Spain). *Environmental Monitoring and Assessment*,
786 136, 3-11.

787 Castell N., Stein A.F., Salvador R., Mantilla E., and Millán M.M., 2008b. The impact of biogenic VOC
788 emissions on photochemical ozone formation during a high ozone pollution episode in the
789 Iberian Peninsula in the 2003 summer season. *Advances in Science and Research*, 2, 9-15.

790 Castell N., Tellez L., and Mantilla E., 2012. Daily, seasonal and monthly variations in ozone levels
791 recorded at the Turia river basin in Valencia (Eastern Spain). *Environmental Science and
792 Pollution Research*, 19, 3461-3480.

793 Cusack M., Pérez N., Pey J., Alastuey A. and Querol X., 2013. Source apportionment of fine PM and
794 sub-micron particle number concentrations at a regional background site in the western
795 Mediterranean: a 2.5 yr study. *Atmos. Chem. Phys.*, 13, 5173-5187.

796 DGT, 2014. Dirección General de Tráfico: Anuario Estadístico General 2014.
797 <http://www.dgt.es/es/seguridad-vial/estadisticas-e-indicadores/publicaciones/anuario-estadistico-general/>

798 Dieguez J.J., Millán M., Padilla L., Palau J.L., 2009. Estudio y evaluación de la contaminación
799 atmosférica por ozono troposférico en España. CEAM Report for the Ministry of Agriculture,
800 Food and Environment, INF FIN/O3/2009. 372 pp. http://www.magrama.gob.es/es/calidad-y-evaluacion-ambiental/temas/atmosfera-y-calidad-del-aire/8_A_Informe_final_ozono-ceam_Julio_2009_tcm7-152609.pdf

801 Dieguez J.J., Calatayud V., Mantilla E., 2014. CEAM Report for the Ministry of Agriculture, Food and
802 Environment, Fundación Biodiversidad. Informe Final. Memoria Técnica Proyecto CONOZE.
803 Contaminación por OZono en España. 137 pp http://www.magrama.gob.es/es/calidad-y-evaluacion-ambiental/temas/atmosfera-y-calidad-del-aire/8_A_Informe_final_ozono-ceam_Julio_2009_tcm7-152609.pdf

807 evaluacion-ambiental/temas/atmosfera-y-calidad-del-
808 [aire/Informe t%C3%A9cnico CONOZE%5B1%5D tcm7-330956.pdf](http://aire/Informe_t%C3%A9cnico CONOZE%5B1%5D tcm7-330956.pdf)

809 Doherty R.M., Wild O., Shindell D.T., Zeng G., Collins W.J., MacKenzie I.A., Fiore A.M., Stevenson, D.S. Dentener, F.J., Schultz M.G., Hess P., Derwent R.G. and Keating T.J., 2013. Impacts of climate change on surface ozone and intercontinental ozone pollution: A multi-model study. *Journal of Geophysical Research* 118, 3744–3763.

810 Doval M., Castell N., Téllez L., and Mantilla E., 2012. The use of experimental data and their uncertainty for assessing ozone photochemistry in the Eastern Iberian Peninsula. *Chemosphere*, 89, 796-804.

811 EC, 2004. European Commission Decision of 19 March 2004 "Concerning guidance for implementation of Directive 2002/3/EC of the European Parliament and the Council relating to ozone in ambient air (2004/279/EC). Oficial Journal of the European Union L87/50 of 25.3.2004.

812 EEA, 2015. Air quality in Europe-2015 report. EEA Report, No 5/2015. ISSN 1977-8449.

813 Escudero M., Lozano A., Hierro J., del Valle J., and Mantilla E., 2014. Urban influence on increasing ozone concentrations in a characteristic Mediterranean agglomeration. *Atmospheric Environment*, 99, 322-332.

814 Gangoiti G., Millán M.M., Salvador R., and Mantilla E., 2001. Long-range transport and re-circulation of pollutants in the western Mediterranean during the project Regional Cycles of Air Pollution in the West-Central Mediterranean Area. *Atmospheric Environment*, 35, 6267-6276.

815 Gangoiti, G., Alonso L., Navazo M., García J.A., Millán, M.M. 2006. North African soil dust and European pollution transport to America during the warm season: Hidden links shown by a passive tracer simulation. *J. Geophys. Res.*, 111, D10109, doi: 10.1029/2005JD005941

816 Geiger R., Aron R.H., 1992. *Todhunter P. The Climate Near the Ground*. Rowman & Littlefield Publishers Inc. 6th Edition. ISBN 0-7425-1857-4, Lonham, Us, 561 pp.

817 Gonçalves M., Jiménez-Guerrero P. and Baldasano J.M., 2009. Contribution of atmospheric processes affecting the dynamics of air pollution in South-Western Europe during a typical summertime photochemical episode. *Atmos. Chem. Phys.*, 9, 849-864.

818 Hertel, O., Skjøth, C.A., Reis, S., Bleeker, A., Harrison, R.M., Cape, J.N., Fowler, D., Skiba, U., Simpson, D., Jickells, T., Kulmala, M., Gyldenkærne, S., Sørensen, L.L., Erisman, J.W. and Sutton, M.A., 2012. Governing processes for reactive nitrogen compounds in the atmosphere, *Biogeosciences*, 9, 4921-4954.

819 Hewson E.W., 1964. *Industrial Air Pollution Meteorology*. Meteorological Laboratories of the College of Engineering. The University of Michigan. Ann Arbor, MI, 191 pp.

820 Kley D., Geiss H., 1994. Tropospheric ozone at elevated sites and precursor emissions in the United States and Europe. *Atmospheric Environment* 8, 1, 149-158.

821 Lee, H.-K., Hwang, I.-K., Ahn, K.-H., 2014. Development and Evaluation of Hy-CPC. *Particle and Aerosol Research* 10, 93-97.

822 Lee, H.-K., Eun, H.-R., Lee, G.-H., Ahn, K.-H., 2015. Development and evaluation of Hy-SMPS, *Particle and Aerosol Research* 11, 57-61.

823 Mantilla E., Millán M.M., Sanz M.J., Salvador R., and Carratalá A., 1997. Influence of mesometeorological processes on the evolution of ozone levels registered in the Valencian Community. In: I Technical workshop on ozone pollution in southern Europe. Valencia.

824 Millán M.M. (Ed.), 2002. *Ozone Dynamics in the Mediterranean Basin: A collection of scientific papers resulting from the MECAPIP, RECAPMA and SECAP Projects*. European Commission (DG RTD I.2) Air Pollution Research Report 78, Available from CEAM, Valencia, Spain, 287 pp.

854 Millán, M.M. 2014. Extreme hydrometeorological events and climate change predictions in
855 Europe. *J. Hydrol.* 518B: 206-224.

856 Millán M.M., Artiñano B., Alonso L., Navazo M., Castro M., 1991. The effect of meso-scale flows on
857 regional and long-range atmospheric transport in the Western Mediterranean area.
858 *Atmospheric Environment* 25A, 5/6, 949-963.

859 Millán M.M., Salvador R., Mantilla E., Artiñano B., 1996a. Meteorology and photochemical air
860 pollution in southern Europe: experimental results from EC research projects. *Atmospheric*
861 *Environment*, 30, 1909-1924.

862 Millán M.M., Mantilla E., Salvador R., Kallos G., 1996b. Regional and long-range transport scenarios
863 for photo-oxidants on the Mediterranean basin in summer. Ninth joint conference on
864 applications of air pollution meteorology. 438-441. American Meteorological Society, Boston.

865 Millán M.M., Salvador R., Mantilla E., 1996c. Mesoscale processes and photo-oxidants cycles on the
866 Spanish Mediterranean coast. Ninth joint conference on applications of air pollution
867 meteorology. 434-437. American Meteorological Society, Boston.

868 Millán M.M., Salvador R., Mantilla E., and Kallos G., 1997. Photooxidant dynamics in the
869 Mediterranean basin in summer: Results from European research projects. *Journal of*
870 *Geophysical Research* 102, 8811-8823.

871 Millán M.M. and Sanz M. J., 1999. Ozone in Mountainous regions and in Southern Europe. In: Ad
872 hoc Working group on Ozone Directive and Reduction Strategy Development, (eds.). *Ozone*
873 *Position Paper*.145-150. European Commission, Brussels.

874 Millán M.M., Mantilla E., Salvador R., Carratalá A., Sanz M.J., Alonso L., Gangoiti G., and Navazo
875 M., 2000. Ozone Cycles in the Western Mediterranean Basin: Interpretation of Monitoring
876 Data in Complex Coastal Terrain. *Journal of Applied Meteorology*, 39: 487-508.

877 Millán M.M., Sanz M.J., Salvador R., and Mantilla E., 2002. Atmospheric dynamics and ozone cycles
878 related to nitrogen deposition in the western Mediterranean. *Environmental Pollution*, 118,
879 167-186.

880 Minguillón M.C., Brines M., Pérez N., Reche C., Pandolfi M., Fonseca A.S., Amato F., Alastuey A.,
881 Lyasota A., Codina B., Lee H.-K., Eun H.-R., Ahn K.-H., Querol X., 2015. New particle formation
882 at ground level and in the vertical column over the Barcelona area. *Atmospheric Research*
883 164-165, 118-130.

884 Monks, P.S., Archibald A.T., Colette A., Cooper O., Coyle M., Derwent R., Fowler D., Granier C., Law
885 K.S., Mills G.E., Stevenson D.S., Tarasova O., Thouret V., von Schneidemesser E., Sommariva
886 R., Wild O., and Williams M.L., 2015. Tropospheric ozone and its precursors from the urban to
887 the global scale from air quality to short-lived climate forcer. *Atmos. Chem. Phys.*, 15, 8889-
888 8973.

889 Palacios M., Kirchner F., Martilli A., Clappier A., Martín F., Rodríguez M.E., 2002. Summer ozone
890 episodes in the Greater Madrid area. Analyzing the ozone response to abatement strategies
891 by modelling. *Atmospheric Environment*, 36, 5323-5333.

892 Pay, M.T., Valverde, V., Baldasano, J.M., Kwok, R., Napelenok, S., Baker, K., 2014.
893 Photochemical Modeling to Attributing Source and Source Regions to Ozone Exceedances in
894 Spain. 13th Annual CMAS Conference, Chapel Hill, NC, October 27-29, 2014. Available at:
895 https://www.cmascenter.org/conference/2014/slides/maria_pay_photochemical_modeling_2014.pptx.

896 Querol X., Alastuey A., Rodríguez S., Plana F., Ruiz C.R., Cots N., Massagué G., Puig O., 2001. PM10
898 and PM2.5 source apportionment in the Barcelona Metropolitan Area, Catalonia, Spain.
899 *Atmospheric Environment* 35/36, 6407-6419.

900 Querol X., Alastuey A., Orio A., Pallares M., Reina F., Dieguez JJ., Mantilla E., Escudero M., Alonso
901 L., Gangoiti G., Millán M. 2016. On the origin of the highest ozone episodes in Spain. *Science of the Total Environment*, 572, 379-389.

903 Rodríguez S., Querol X., Alastuey A., Mantilla E., 2002. Origin of high summer PM10 and TSP
904 concentrations at rural sites in Eastern Spain. *Atmospheric Environment* 36, 3101-3112.

905 Salvador R., Millán M.M., and Calbo J., 1999. Horizontal Grid Size Selection and its influence on
906 Mesoscale Model Simulations. *Journal of Applied Meteorology*, 38, 1311-1329.

907 Salvador R., Millán M.M., Mantilla E., and Baldasano J.M., 1997. Mesoscale modelling of
908 atmospheric processes over the western Mediterranean area during summer. *International
909 Journal of Environment and Pollution*, 8, 513-528.

910 Seco R., Peñuelas J., Filella I., Llusia J., Molowny-Horas R., Schallhart S., Metzger A., Müller M.,
911 Hansel A., 2011. Contrasting winter and summer VOC mixing ratios at a forest site in the
912 Western Mediterranean Basin: the effect of local biogenic emissions. *Atmospheric Chemistry
913 and Physics* 11, 13161-13179.

914 Skamarock W.C., Klemp J.B., Gill D.O., Barker D.M. and J.G. Powers, 2008. A description of the
915 advanced research WRF version 3.NCAR. Tech. Note NCAR/TN-468+STR, 88pp. NCAR:
916 Boulder, Colorado, USA.

917 Soler, M.R.; Hinojosa, J., Bravo, M., Pino D., Vilà Guerau de Arellano, J., 2004. Analyzing the basic
918 features of different complex terrain flows by means a Doppler Sodar and a numerical model:
919 Some implications to air pollution problems. *Meteorology and Atmospheric Physics*, 1-3,
920 141,154.

921 Soler M.R., Arasa, A., Merino M., Olid M. and Ortega S., 2011. High vertical resolution numerical
922 simulation of the sea-breeze flow in Catalonia. Implications to spatial and temporal variability
923 of ozone and PM10 levels. *Bound.-Layer Meteor*, 140, 37-56.

924 Soler R.M., Gámez P. and Olid M., 2015. Aramis a regional air quality model for air pollution
925 management: evaluation and validation. *Física de la Tierra*, 27, 111-136

926 Stein A.F., Mantilla E., and Millán M.M., 2004. Ozone formation downwind an industrial complex in
927 the western Mediterranean. In: 13th World Clean Air and Environmental Protection. August
928 22-27. London, U.K.

929 Stein A.F., Mantilla E., and Millán M.M., 2005. Using measured and modelled indicators to assess
930 ozone-NOx-VOC sensitivity in a western Mediterranean coastal environment. *Atmospheric
931 Environment*, 39: 7167-7180.

932 Tang Y.S., Cape J.N., Sutton M.A., 2001. Development and types of passive samplers for NH₃ and
933 NOx. In: Proceedings of the International Symposium on Passive Sampling of Gaseous
934 Pollutants in Ecological Research. Science World, vol. 1, pp. 513-529.

935 Toll, I., Baldasano, J.M., 2000. Modeling of photochemical air pollution in the Barcelona area with
936 highly disaggregated anthropogenic and biogenic emissions. *Atmos. Environ.* 34, 3069-3084.

937 UNECE, 2010. Hemispheric transport of air pollution 2010. Part A: ozone and particulate matter. Air
938 pollution studies, 17. UNECE, LRTAP, Task Force on Hemispheric Transport of Pollutants HTAP
939 2010: Part A. Ozone and Particulate Matter, 278 pp, ECE/EB.AIR/100, ISBN 978-92-1-117043-6
940 http://www.htap.org/publications/2010_report/2010_Final_Report/HTAP%202010%20Part%20A%2020110407.pdf

942 Valverde V., Pay M.T., Baldasano J.M., 2016. Ozone attributed to Madrid and Barcelona on-road
943 transport emissions: Characterization of plume dynamics over the Iberian Peninsula. *Science of the Total Environment* 543, 670-682.

945

946 **FIGURE AND TABLE CAPTIONS**

947 Figure 1. Top: Study area and location of monitoring sites (regional air quality monitoring sites
948 XVPCA, dosimeters, meteorological stations and vertical measurements). BMA: Barcelona
949 Metropolitan Area. Bottom: Topographic profiles across the study area, red arrows point to the
950 valleys connecting BMA with the Vic Plain and the Pre-Pyrenean regions.

951 Figure 2. Geopotential and temperature at 850 hPa (left) and 500 hPa (center). Potential
952 temperature (K) of the atmospheric sounding in Barcelona (WMO 08190) at 12:00 UTC (right).
953 Meteorological figures are reported for 03/07/2015 (top) and 14/07/2015 (bottom).

954 Figure 3. Data from the non-tethered balloon measurements (at VIC) of temperature, relative
955 humidity, and particle number concentrations performed from 10:00 to 11:30 UTC on 16/07/2015.
956 Red lines identifies the limit between different atmospheric layers.

957 Figure 4. Top: Mean hourly (UTC) values for meteorological parameters and O₃ ambient air
958 concentrations measured during 03-06, 14-20 and 10-17/7/2015 recorded at the permanent VIC
959 XVPCA station (O₃) and at the Gurb meteorological station (temperature, humidity and wind
960 patterns, Meteocat) located 1 km to the north of Bottom: Mean hourly concentrations of other
961 gaseous and particulate pollutants measured at VIC with the laboratory van (only during 10-
962 17/07/2015) co-located with the XVPCA station.

963 Figure 5. O₃ hourly concentrations recorded at the coastal (BEG, blue) and remote inland western
964 pre-Pyrenean (MSC, clear green, 1570 m a.s.l.) sites, 2 urban background sites of Barcelona (PLR,
965 CTL, grey and black), 2 urban sites in the northern periphery of the Barcelona's metropolitan area
966 (GRA, MON, orange and yellow), the inner Vic Plain sites (TON, VIC and MAN, red, pink and violet)
967 and the remote eastern pre-Pyrenean site of PAR (brown), along July 2015.

968 Figure 6. Polar plots of hourly O₃ concentrations in the real-time measurement sites.

969 Figure 7. O₃ and O_x (O₃+NO₂) hourly concentrations recorded at the coastal (BEG, blue, at this site
970 only O₃ is available due to the lack of NO₂ measurements), an urban background site of Barcelona
971 (CTL, black), an urban site in the northern periphery of the Barcelona's metropolitan area (GRA,
972 orange), the intermediate inland rural site of MSY (720 m a.s.l., green), and the inner Vic Plain site
973 (TON, red) along July 2015. The pink and blue squares mark the A and B O₃ and O_x episodes
974 distinguished in this study, respectively.

975 Figure 8. Mean hourly levels of O₃ and O_x (O₃+NO₂) for sites in a south (coast) to north (inland)
976 transect (CTL, GRA and BEG, and MSY, TON, VOIC, MAN and PAR, respectively) following the inland
977 transport of pollutants from the coast, and maxima time shift according to the sea breeze
978 transport (right) for the periods 3-6/07/2015 (B type episode, left) and 14-20/07/2015 (A type
979 episode, right). Time is UTC.

980 Figure 9. Top: Hourly O₃ maxima (and number of hours exceeding 180 µg/m³) in the study sites
981 with real time O₃ measurements (shadowed areas indicate 2 different degrees of exceedances, 1-3

982 h and 13-23h). Bottom: Frequency of occurrence of hourly (UTC) O_3 exceedances of $180 \mu\text{g}/\text{m}^3$
983 along the day; both for July 2015.

984 Figure 10. Vertical profiles of particle number concentrations for particles $>3 \text{ nm}$ (red, N_3), $0.3\text{-}0.5$
985 μm (blue, $\text{PM}_{0.3\text{-}0.5}$), $0.5\text{-}1.0 \mu\text{m}$ (maroon, $\text{PM}_{0.5\text{-}1}$) and wind direction obtained with the tethered
986 balloon measurements on 14 and 17/07/2015.

987 Figure 11. Vertical profiles of O_3 , temperature and relative humidity obtained with the tethered
988 balloon measurements on 14 and 17/07/2015.

989 Figure 12. Time variation of altitude, temperature, relative humidity, N_3 , particle number size
990 distributions and O_3 concentrations during the tethered balloon measurements on 16/07/2015. 1
991 to 3 illustrate the nucleation episode recorded at surface level with particle number size
992 distributions, and 4 the typical regional background N size distribution at around 300 m over the
993 ground.

994 Figure 13. Vertical profiles of BC (5 min time resolution) and O_3 (10 seconds time resolution) at
995 VIC.

996 Figure 14. Mean hourly O_3 concentrations, and wind speed and wind direction for the episodes A
997 and B, showing higher levels in the A episodes for the two O_3 maxima.

998 Figure 15. Maps of simulated NO_2 and O_3 concentrations at ground level and 1000m a.g.l., and
999 horizontal wind fields at 10 m a.g.l. for selected hours on 03/07/2015.

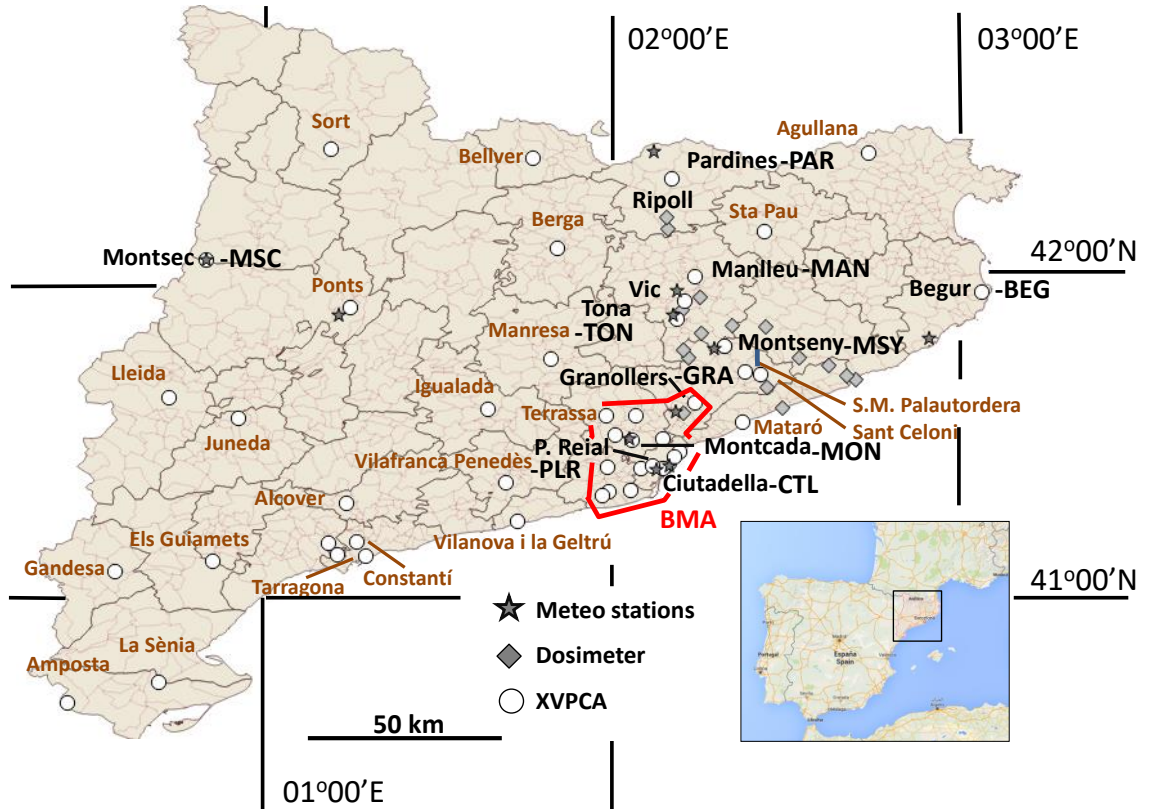
1000 Figure 16. Maps of simulated NO_2 and O_3 concentrations at ground level and 1000m a.g.l., and
1001 horizontal wind fields at 10 m a.g.l. for selected hours on 15/07/2015.

1002 Figure 17. Spatial distributions of simulated O_3 concentrations and wind field vectors in the south–
1003 north vertical cross-section for different hours on 03 and 15/07/2015.

1004

1005

1006



1007

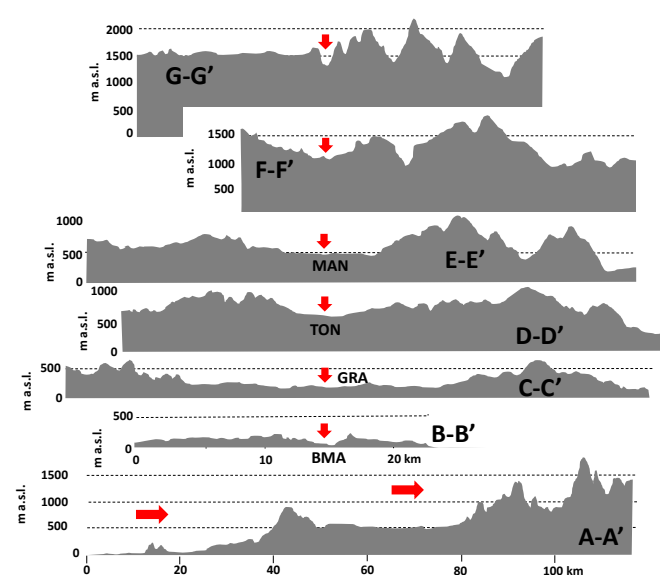
1008

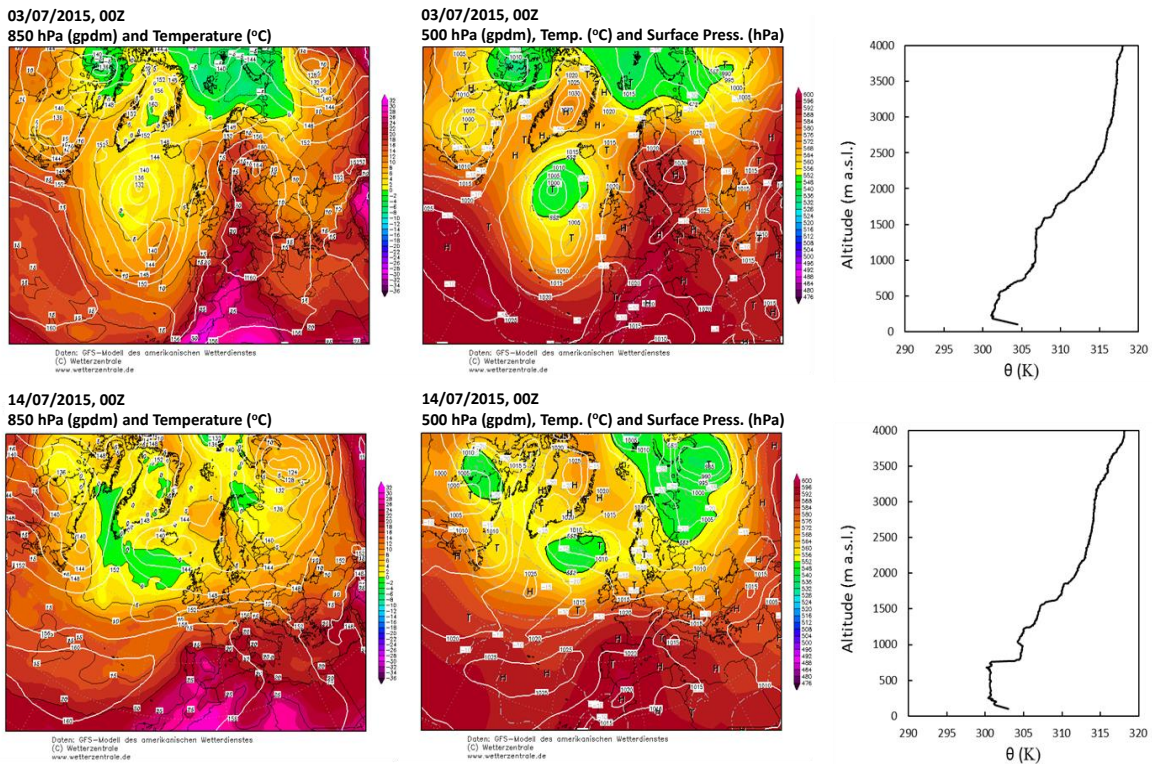
1009

1010

1011

Figure 1

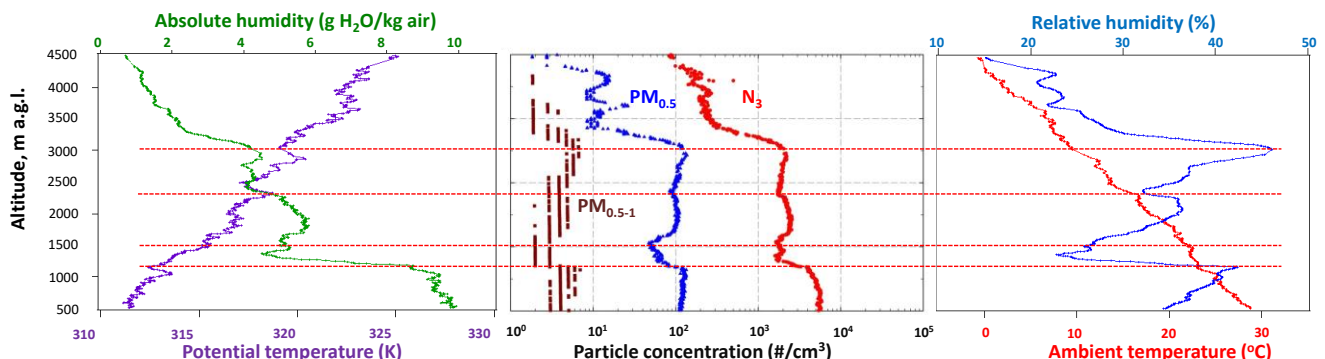




1012

1013 Figure 2.

1014



1015

1016 Figure 3.

1017

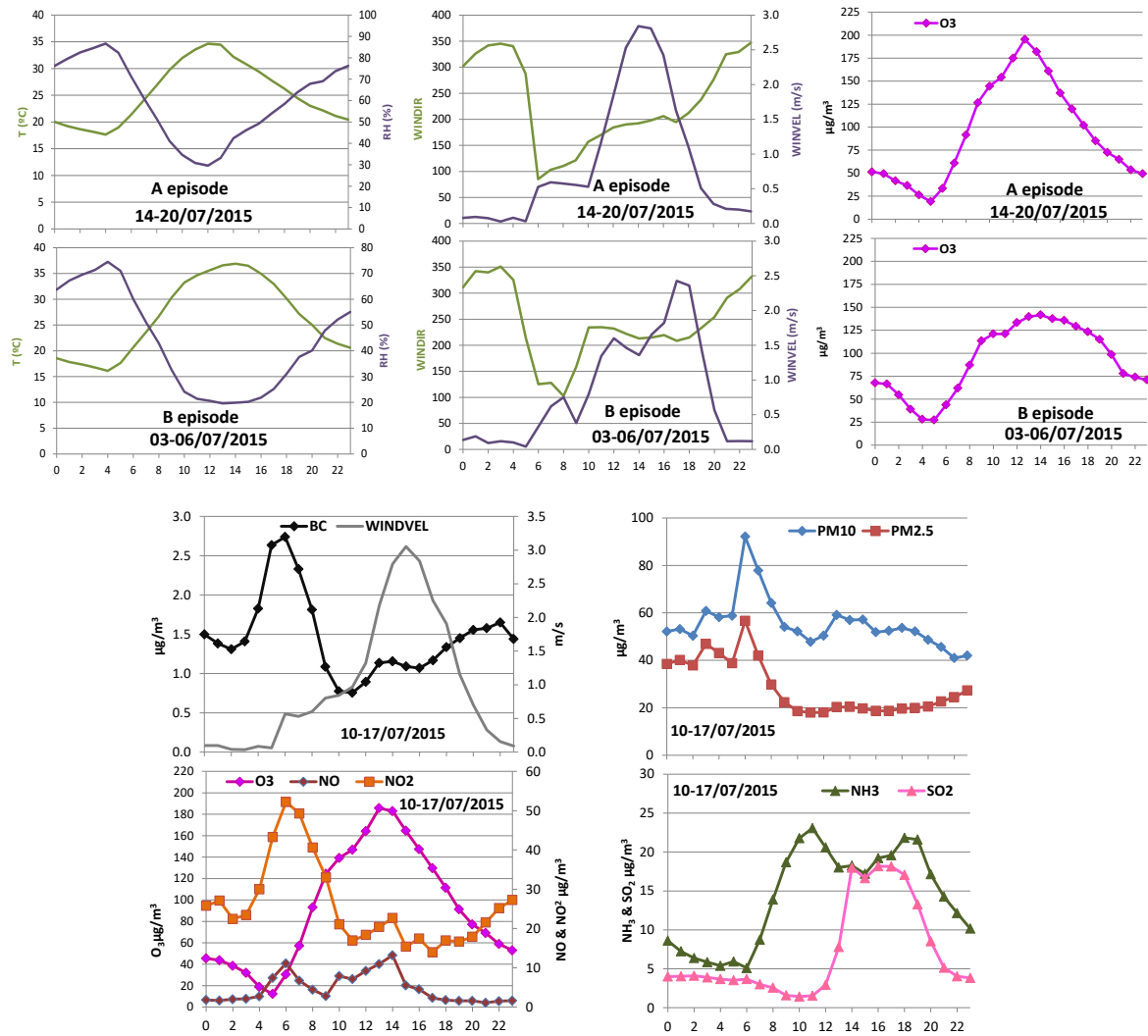


Figure 4

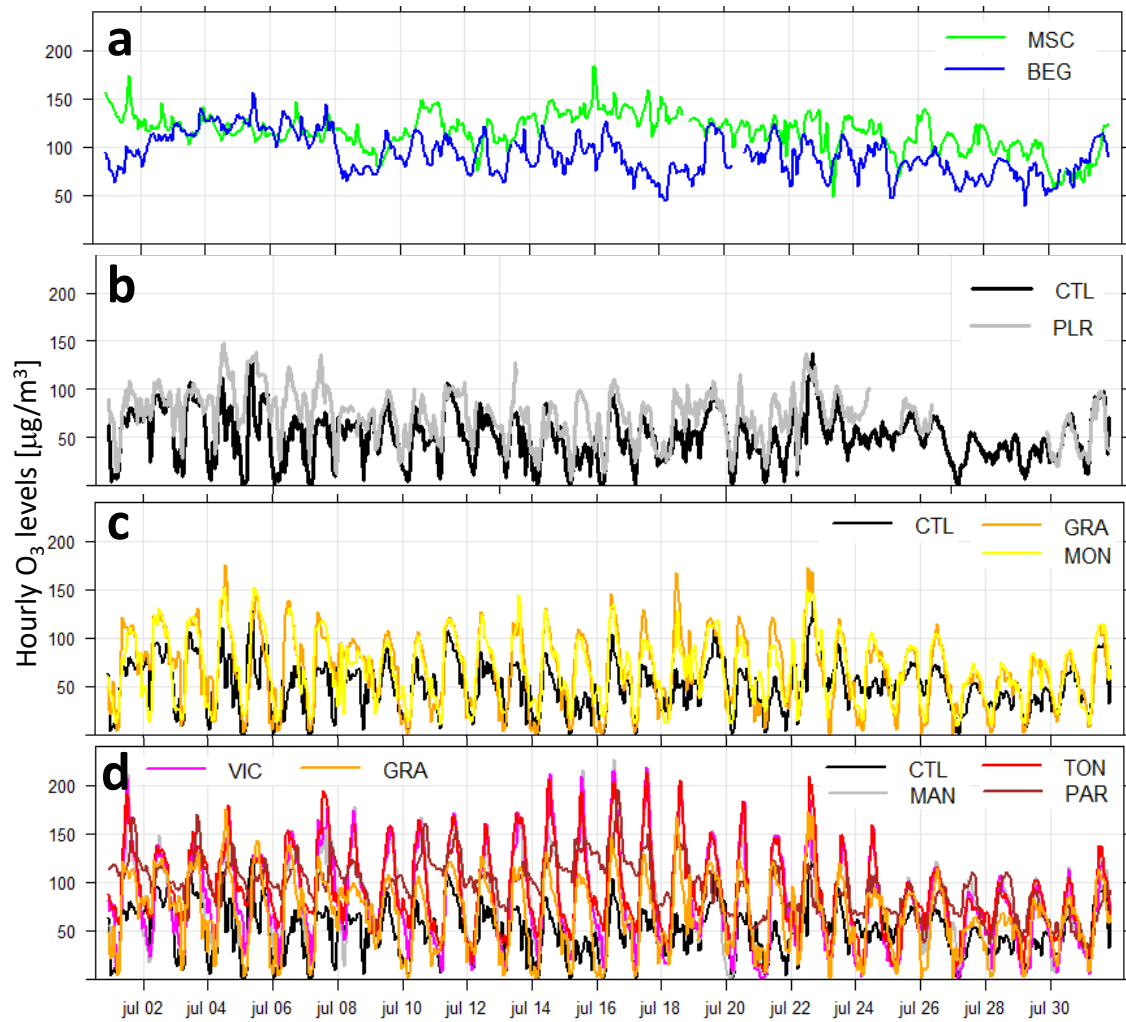


Figure 5

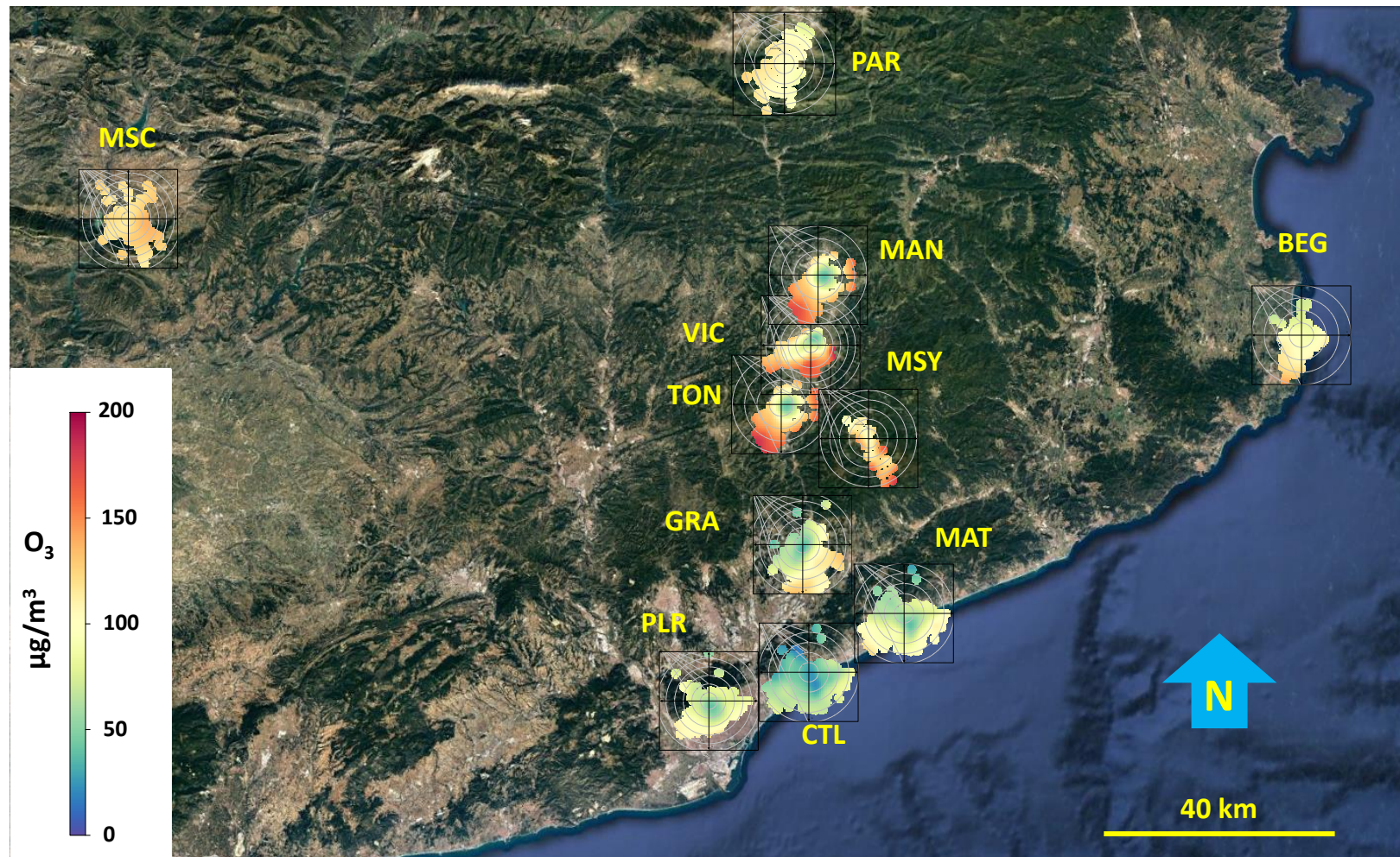


Figure 6

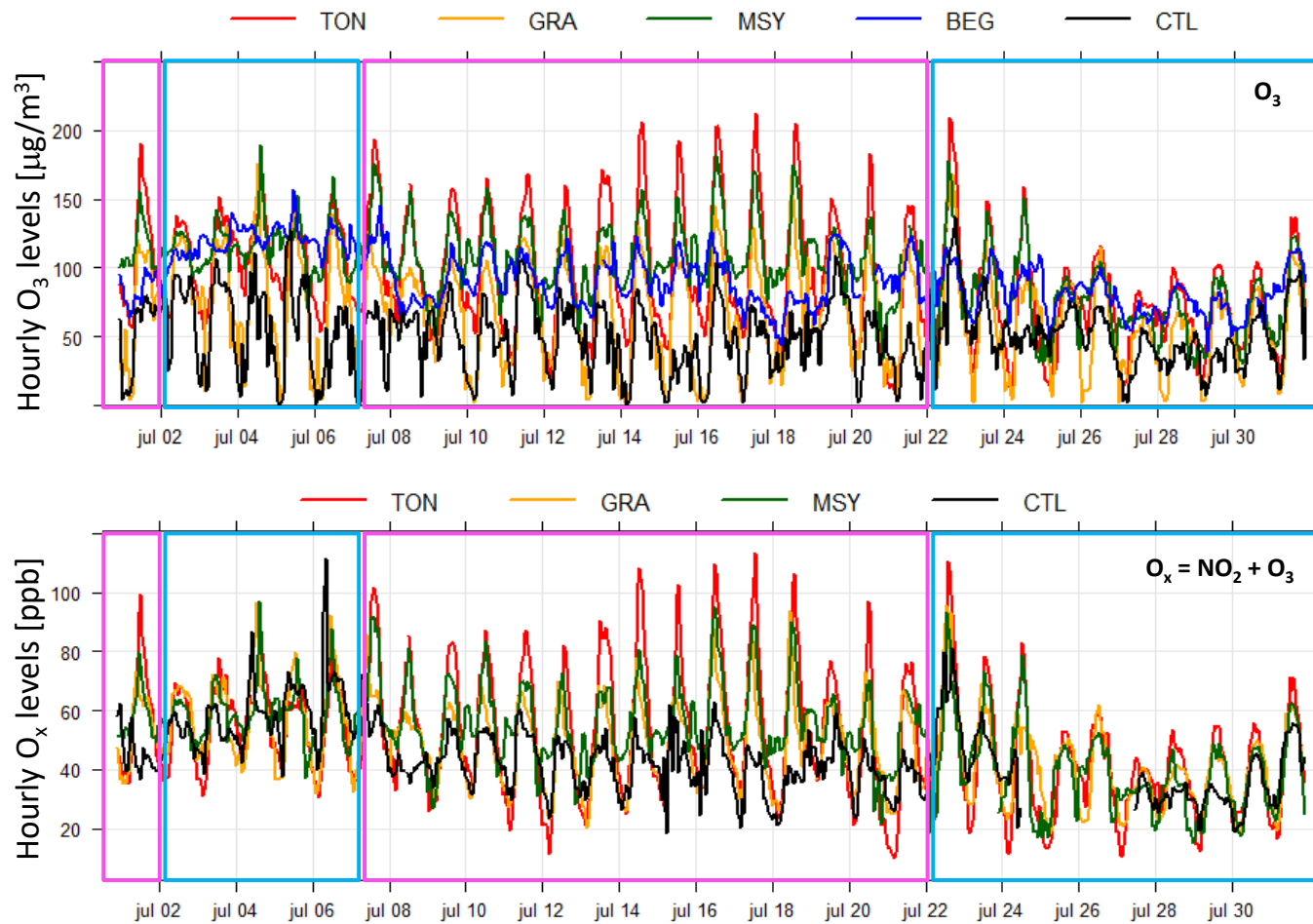


Figure 7.

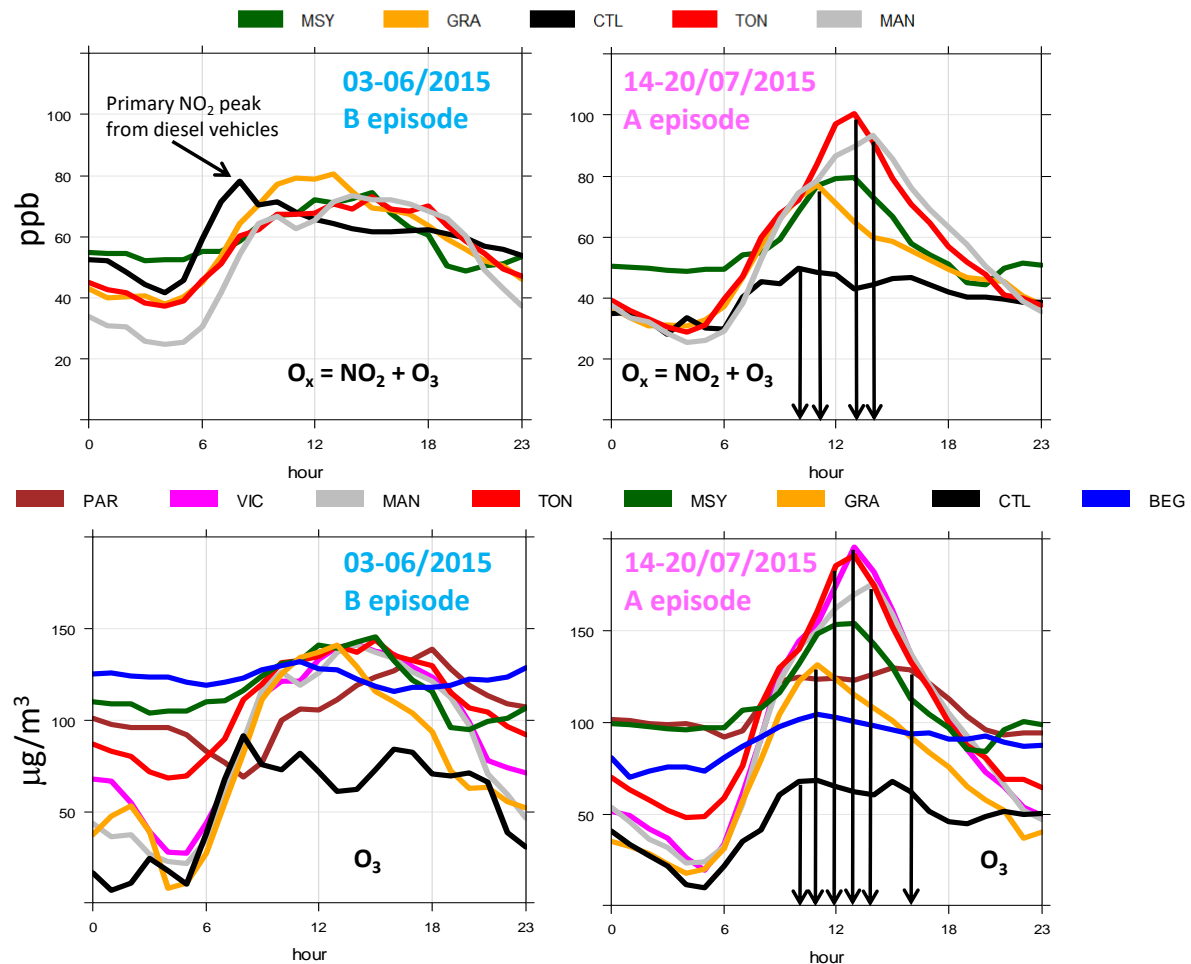


Figure 8.

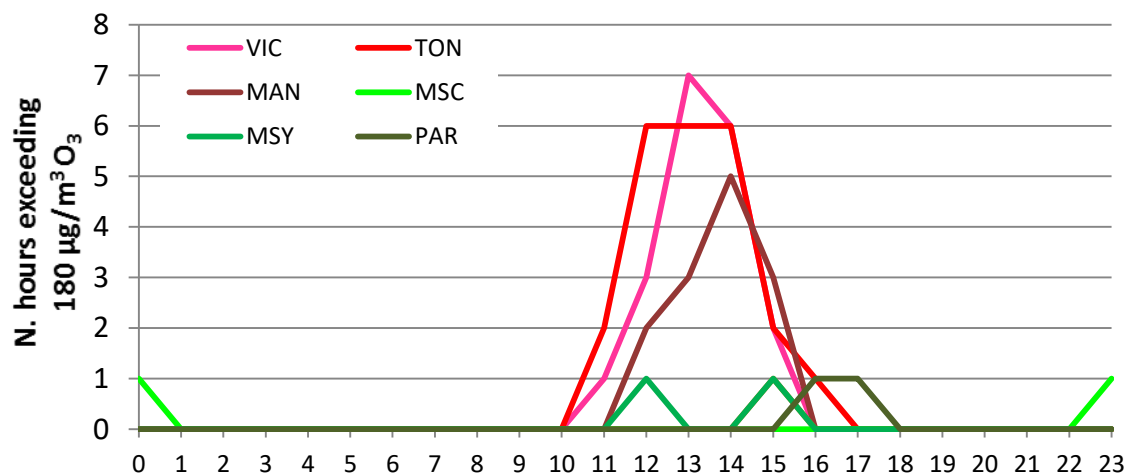
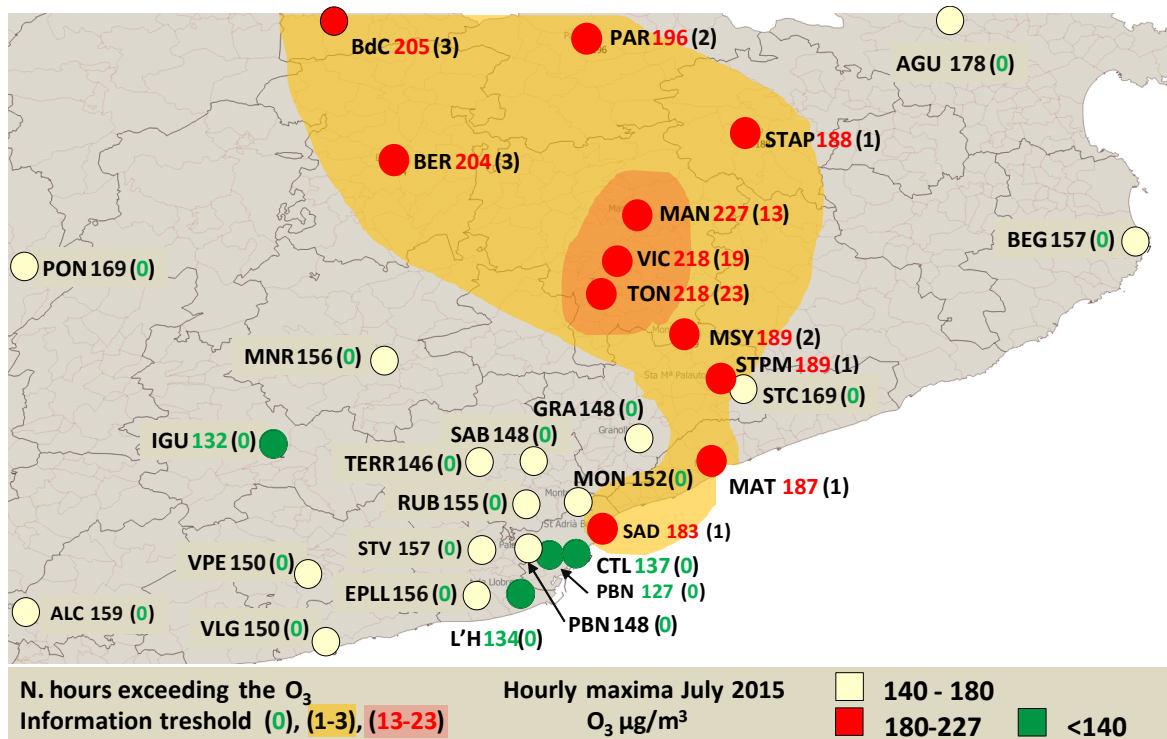


Figure 9.

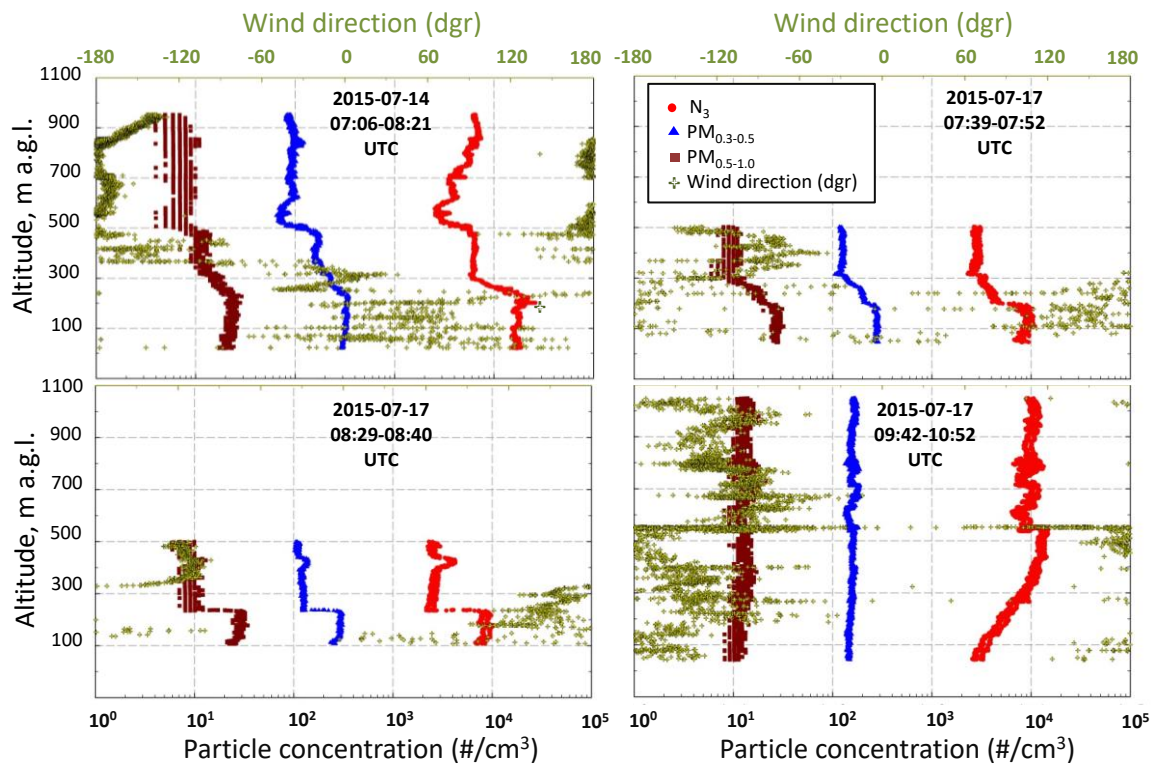


Figure 10.

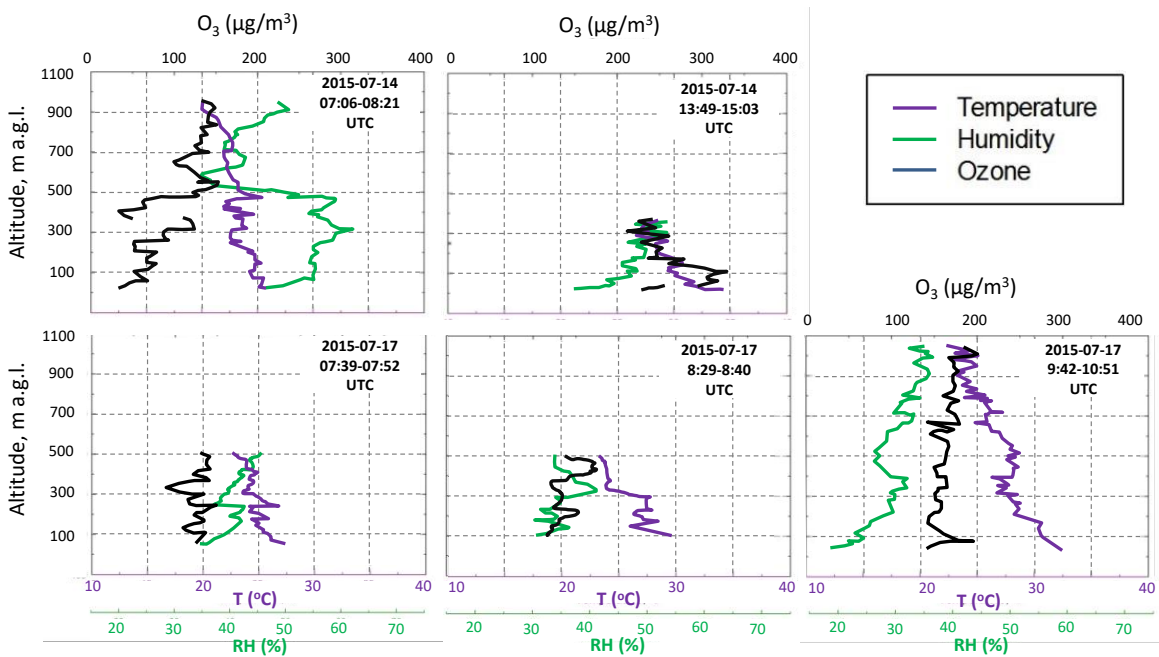


Figure 11

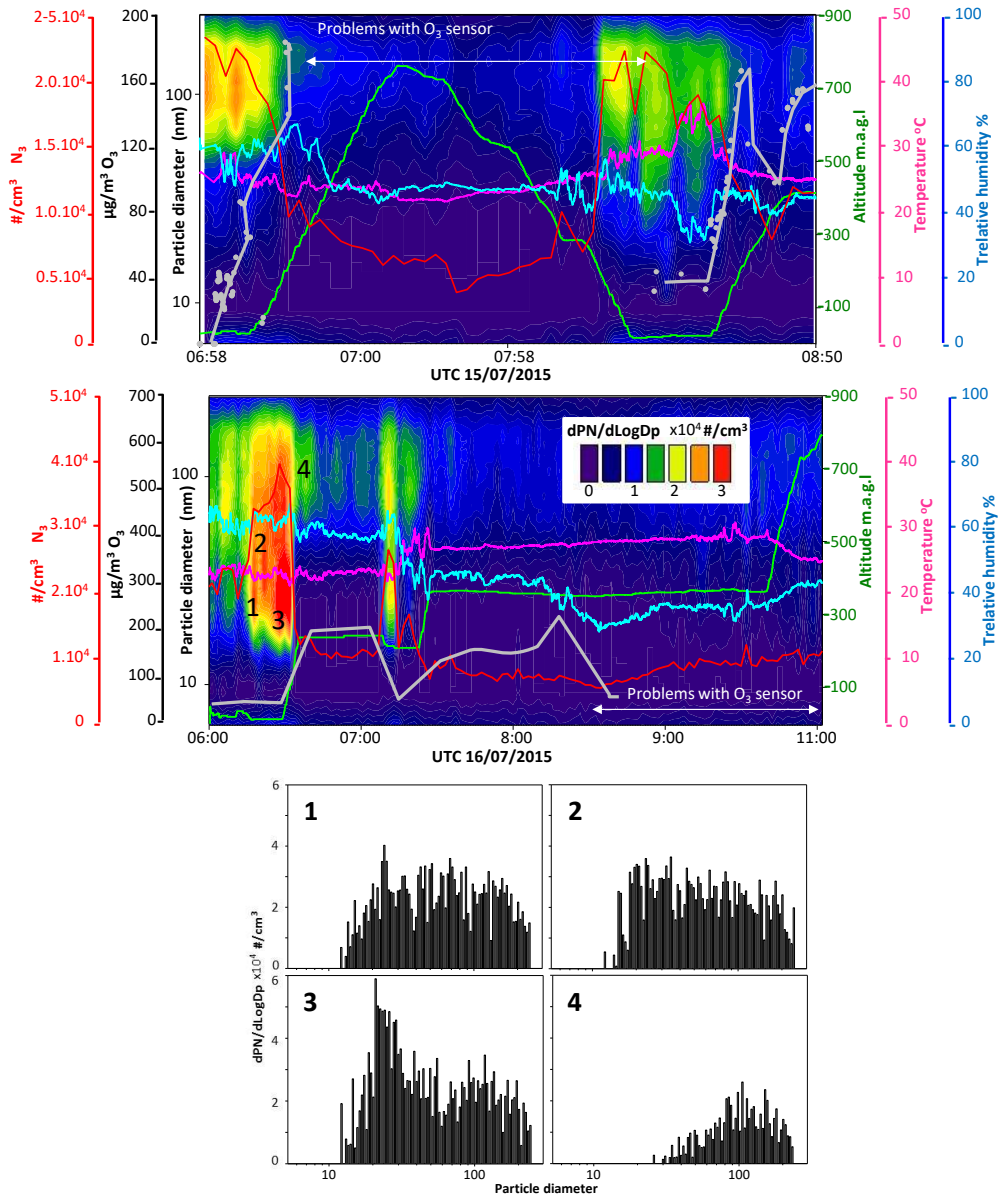


Figure 12

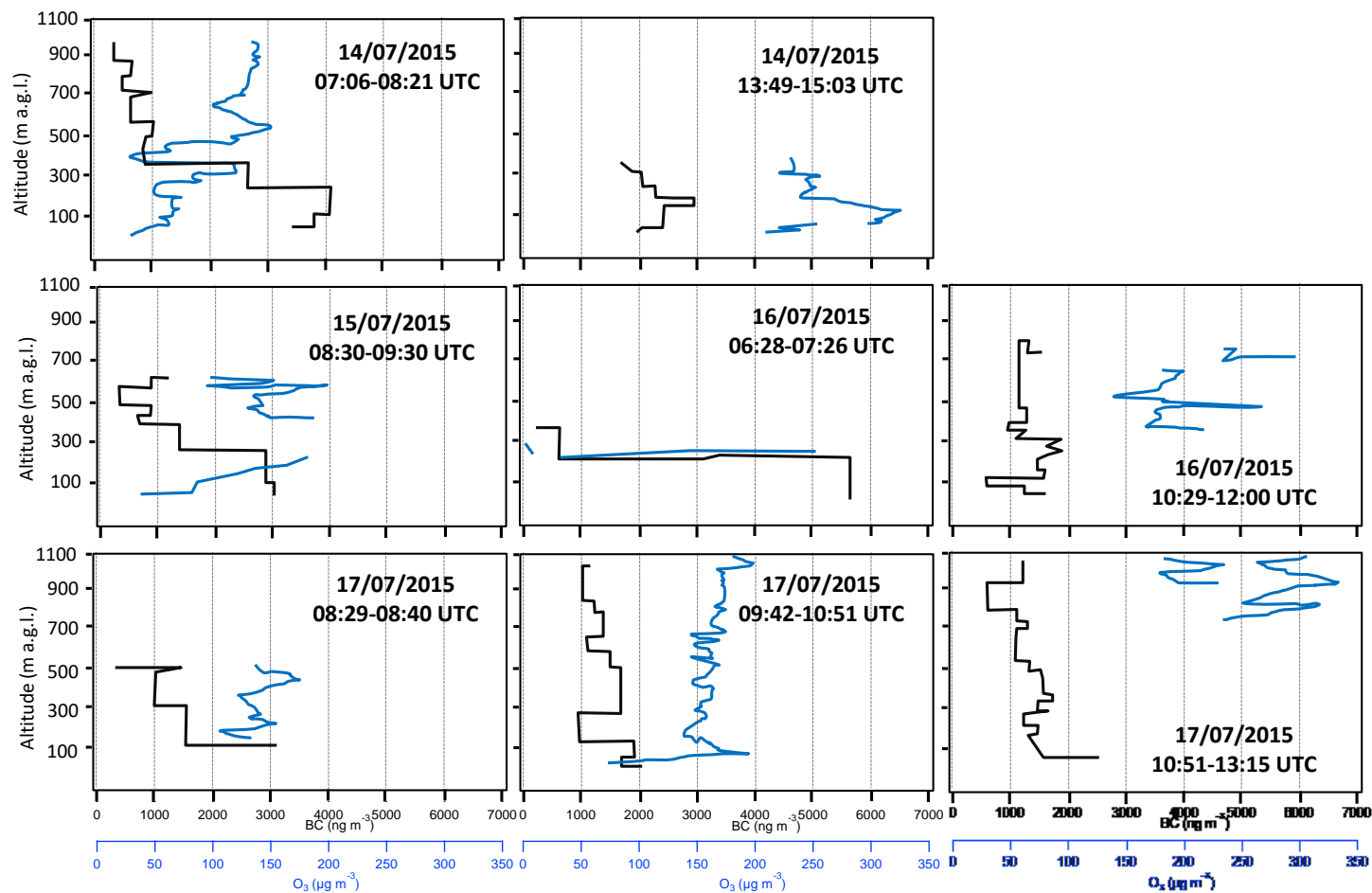


Figure 13

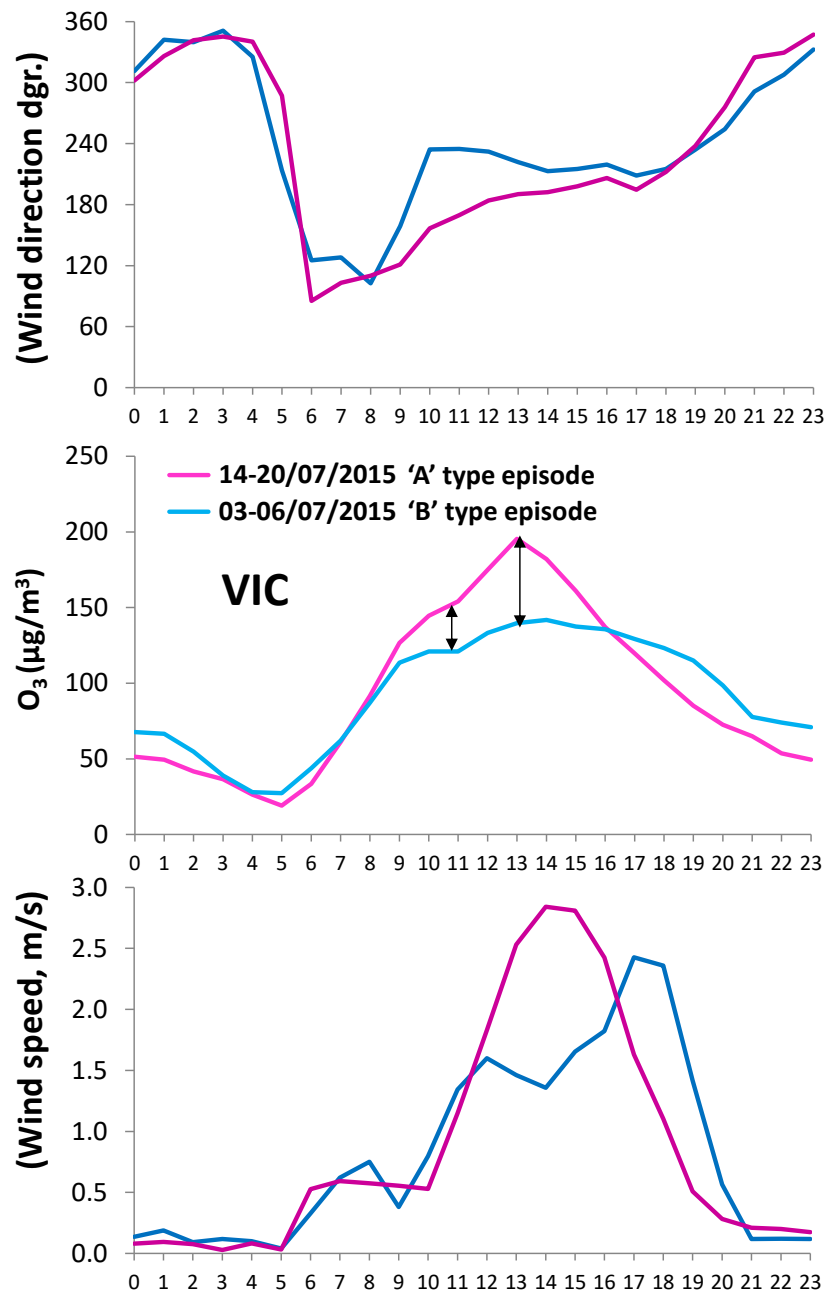


Figure 14

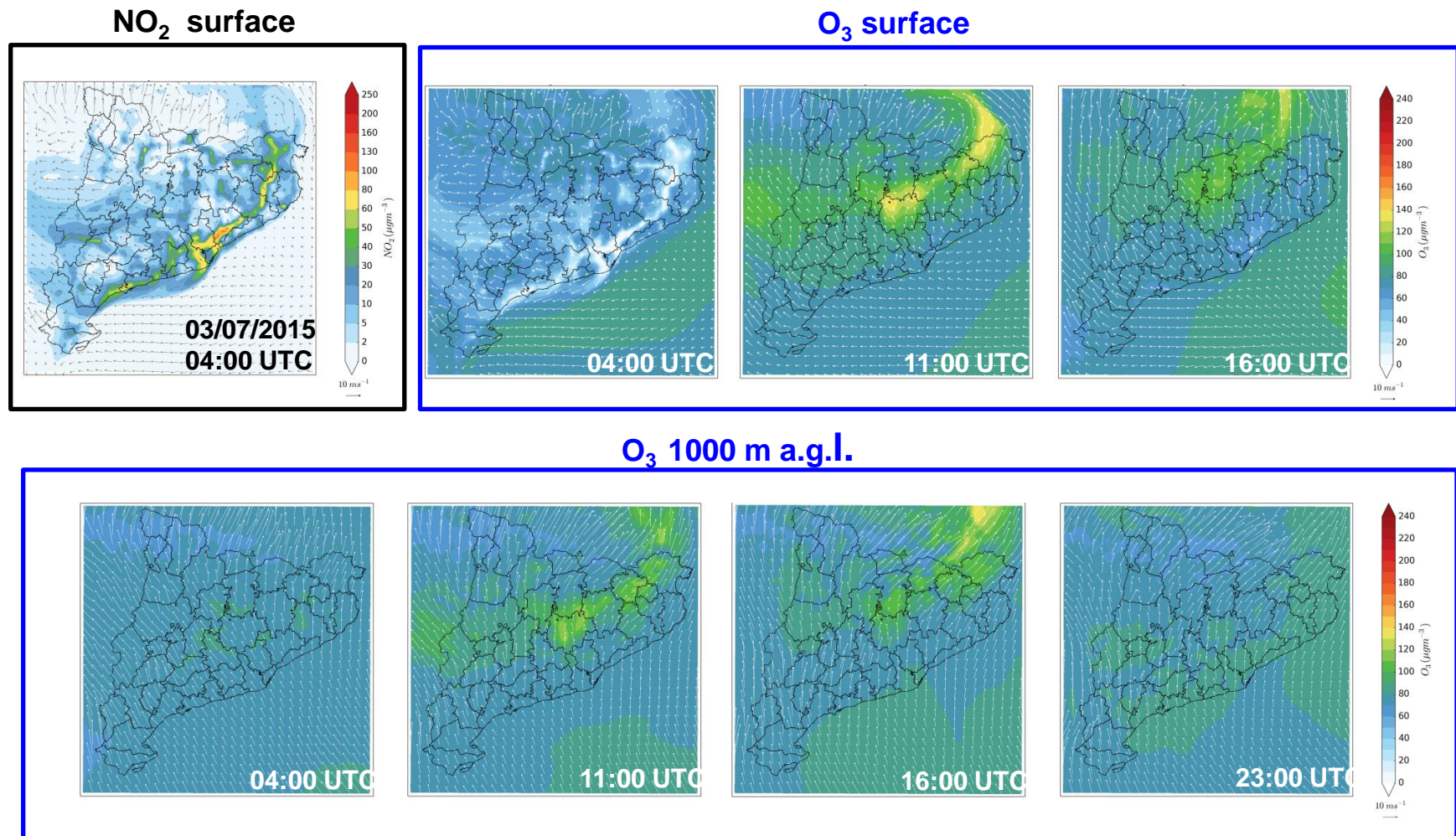


Figure 15

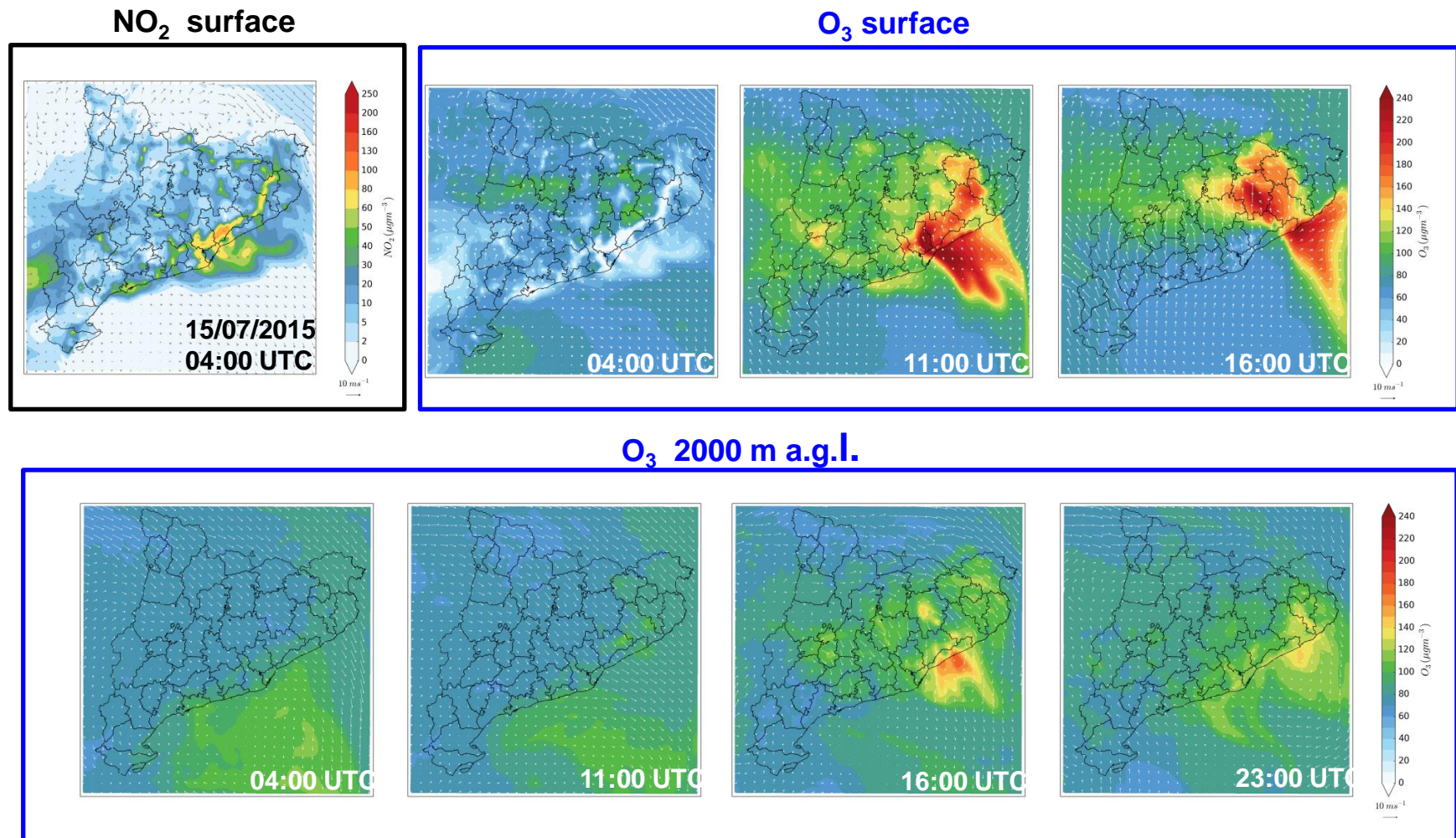


Figure 16

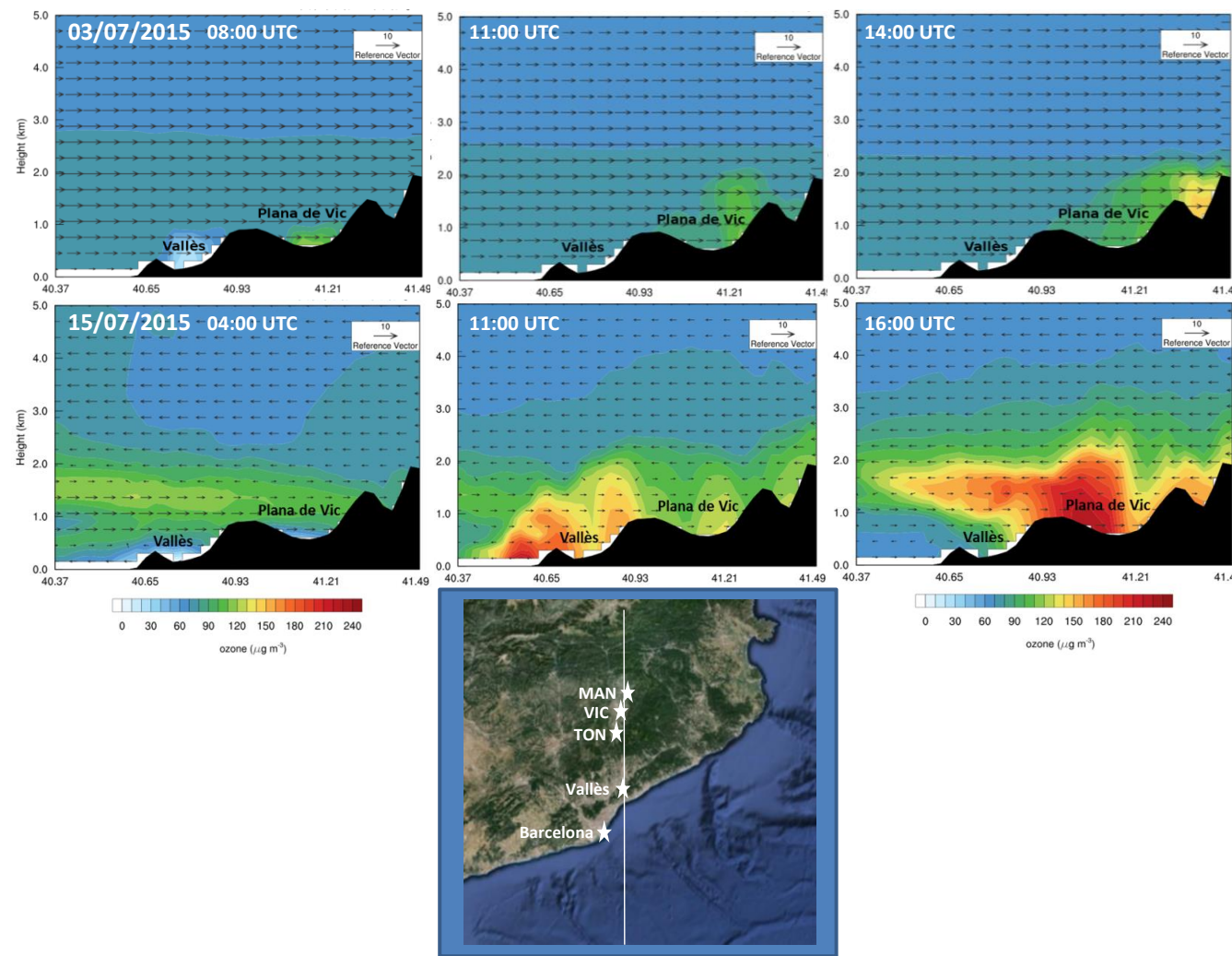


Figure 17